Open Access

Journal of Energy and Power Technology

LIDSEN Publishing Inc.

Original Research

Array Formation Testing with Multiple Azimuthal and Axial Pressure Transducers

Minggao Zhou [1], Yongren Feng [1], Yongzeng Xue [1], Yanmin Zhou [1], Yongchao Chen [1], Wilson C. Chin [2, *]

1. China Oilfield Services Limited (COSL), Beijing, China; E-Mail: zhoumg2@cosl.com.cn; fengyr@cosl.com.cn; xueyz@cosl.com.cn; zhouym3@cosl.com.cn; chenych23@cosl.com.cn
2. Stratamagnetic Software, LLC, Houston, Texas, USA; E-Mail: stratamagnetic.software@outlook.com

* **Correspondence:** Wilson C. Chin; E-Mail: stratamagnetic.software@outlook.com

Academic Editor: Grigorios L. Kyriakopoulos

Journal of Energy and Power Technology
2023, volume 5, issue 4
doi:10.21926/jept.2304038

Received: April 12, 2023
Accepted: November 19, 2023
Published: November 27, 2023

Abstract

An early formation tester operating a “sink probe” that extracts fluids from the borehole, also measures pressures at its location; pressures are additionally collected at two passive sensors, one situated 180 deg away and the second about meter axially. These positions are not conducive to accurate permeability predictions, since pressure transient signals used for inverse analysis attenuate very rapidly. Closer probe spacings offer formation evaluation advantages at low mobilities because Darcy pressure dissipation is reduced. Logging applications for such testing tools include heterogeneity, anisotropy and layer characterization. Multiprobe tools with smaller transducer separations are ideal, but at present, analytically based hardware design and software interpretation methods are not available. Two design approaches are described in this paper, namely, testers with multiple probes that are displaced azimuthally, and those with axially displaced probes. For the former, we describe a new triple-probe array tester and related software models that support pressure transient analysis in transversely isotropic media. The numerical approach supports independently operable probes with different nozzle shapes, flow rates and start and stop times. This flexibility supports anisotropy and heterogeneity mapping

circumferentially about the borehole. The latter class of tools, those formed by axial pressure arrays, extend conventional “dual probe tools” by including additional pressure probes axially along the same azimuth. These support improved pressure gradient analysis and detection of isolated zones in vertical wireline applications. Taken together, both array methods and their computational models support more effective job planning and inverse properties analysis. Comments are also offered on “hybrid multiprobe tools” consisting of both azimuthal and axial arrays. These math formulations and computing methods for both tool classes not only support pressure analysis, but also, for more effective hardware design. For example, what pump flow rates are required to provide a given depth of investigation? Analogous questions can be answered “on paper” prior to prototype building. Representative computed examples are presented demonstrating the versatility and capabilities of the new models. This article introduces techniques focusing on single-phase flow fundamentals. Applications to other multiprobe tools, together with multiphase extensions, dealing with coupled pressure and contamination models, nonlinear gas pumping, convergence acceleration, and in addition, inverse approaches and “big data” support, will be presented in a forthcoming 2024 book.

Keywords
Anisotropy; buildup; compressibility; drawdown; formation testing; MDT; multiprobe; ORA; permeability; pore pressure; pressure gradient; pressure transient analysis; reservoir characterization; Saturn; well testing.

1. Tool Descriptions and Background

Formation testers are borehole measurement devices whose nozzles extract in situ fluids from underground rock using retracting pistons for surface analysis. Darcy pressure transients are monitored and properties like permeability, anisotropy and compressibility are predicted from special software interpretation models or “inverse models.” This is often not possible with earlier dual probe tools alone. There is an industry need for multiprobe tools, together with new simulators based on rigorous mathematics and physical principles.

1.1 Prior Formation Testing Tools

Earlier 1990s devices, which still see commercial application, consist of single “pumping” probes, also known as single “source” or “sink probes.” These terms are used interchangeably, referring to formation testers whose single probes serve both a pumping function and one that passively measures and records pressure. In addition to “single-probe tools,” “dual-probe tools” are also available, in which an additional passive observation probe a small axial distance away records pressure. Pressure data from the former will predict $k_h^{2/3}k_v^{1/3}$ at best, while that from the latter will yield k_h and k_v individually using inverse math models and appropriate software. Despite their importance, these tools will not offer properties along the circumference of the well. To obtain azimuthal borehole information, newer multiprobe tools are required.

1.2 Newer Multiprobe Tools

To obtain geological information over larger spatial scales, multiple probes are required. Additional probes decrease the spacing between adjacent probes, so that pressure attenuation in low mobility formations is less of a problem. Here we will consider two types of "array formation tester" concepts, with each supporting multiple transducers. The first assumes sensors distributed azimuthally around the tool, while the second focuses on axially distributed sensors placed along the same azimuth as the "sink" probe. Azimuthal arrays are discussed first, while axial arrays will be described in the second portion of this paper. The math models developed for both concepts will be summarized here, and it is clear that different hybrid hardware designs are possible by mixing azimuthal and axial transducer combinations.

For readers interested in field applications and mathematical details, refer to Chin et al., Chin et al. and Chin [1-3] for single-probe tools, and to Lu et al., Lu et al. and Chin [4-6] for the newer azimuthal multiprobe tools, e.g., Schlumberger's Saturn™ and ORA™, COSL's "triple probe", and Halliburton and Baker patented concepts in Proett and Bonavides [7] and Morgan et al. [8], respectively. The present paper provides a concise review of azimuthal and axial array tools, and insights into how the two types of probes might be combined in a more versatile hardware device. As Chin [6] (now, in press) is not presently available, the author will provide a complimentary draft version upon request.

1.3 Azimuthal Versus Axial Multiprobe Tools - Pictorial Illustrations

For azimuthal tools, a "three arm" multiprobe tester is described with three independently operable sink probes located at 120 deg separations. Analysis shows that four-probe tools do not offer improved physical resolutions justifiable by hardware and reliability complications. In fact, improved formation evaluation accuracy can be achieved using higher pumping rates. In our design, each probe may operate independently or in unison. This provides flexibility in directional azimuthal logging. The "three arm" tool may contain mixed nozzles which may be small, round or oval, and long and slotted, thus accommodating a wide range of formation types from standard matrix rocks to natural fractures and unconsolidated sands, as shown in Figure 1.

1.3.1 Azimuthal Probe Formation Tester

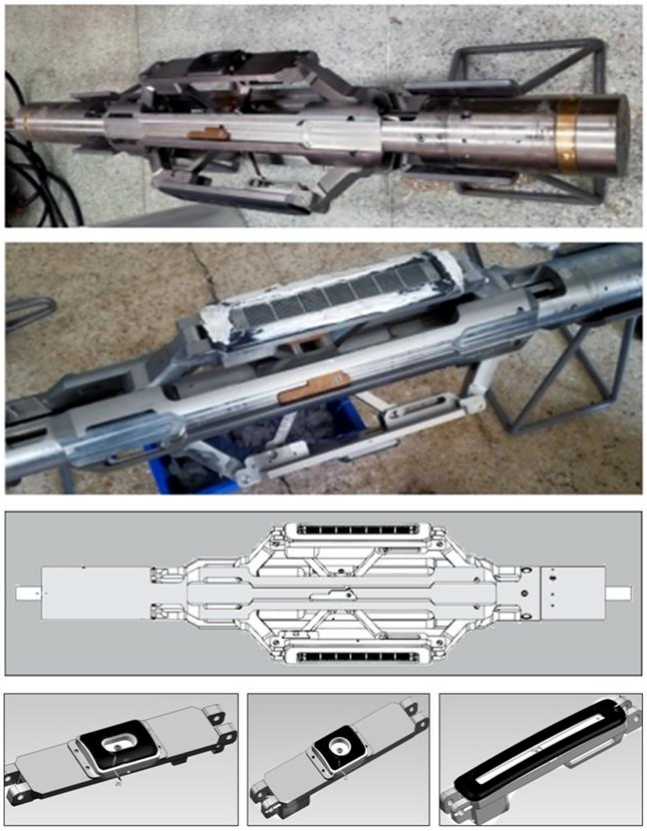

Figure 1 Azimuthal tester – (a) Top two photos, fluid withdrawal from the formation using “small round nozzles” (upper) and “lengthy slotted nozzles” (lower); (b) Middle drawing, long slot nozzles, detailed mechanical assembly; and (c) Bottom drawings, multiple pad varieties support broad pump rate, formation types and permeability/viscosity ranges.

1.3.2 Axial Probe Formation Tester

Azimuthal and axial tools accommodate all formations, including unconsolidated sands and fractured rocks. Different nozzle areas support a wide range of withdrawal rates in various permeability scenarios, so that large pressure declines, undesirable gas release and excessive power requirements can be avoided. These features also motivated development of simulation methods covering a broad range of reservoir applications, including heterogeneity, anisotropy and layer characterization, and also pressure gradient analysis. For axial tools, Figure 2 shows a lineal axial assemblage of pressure transducers used to support detailed vertical analysis, anisotropy mapping in thick layers and pressure gradient studies. Figure 3 offers a resolution/depth schematic similar to those used in electrical or electromagnetic array logging.

Figure 2 Axial tester - Scanning “array formation tester” concept also provides multiple depths of investigation with different lateral resolutions.

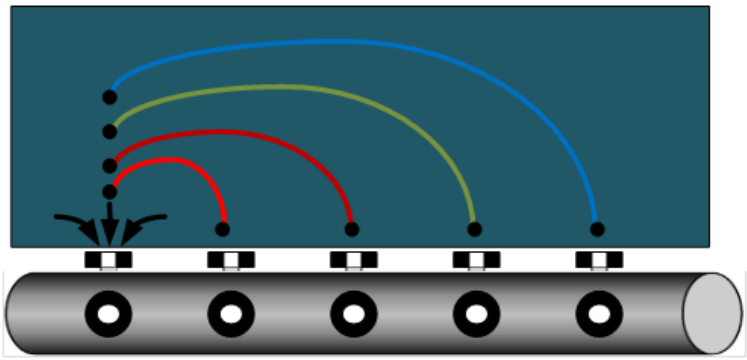

Figure 3 Axial tester - High resolution, low investigation depth for small probe separations; low resolution, high investigation depth for large probe separations.

While numerical simulations, which will discussed in Section 2, provide useful design and analysis guidance, experimental checks are always necessary. Flow evaluation lab facilities supporting large diameter cores like those illustrated in Figure 4 and Figure 5 fulfill these requirements in COSL efforts. Experimental findings are typically incorporated into software models, for instance, using empirical geometric factor corrections and calibrations that account for pad geometry and sealing effects. For additional details related to COSL test fixture design and core sample preparation for Figure 4 and Figure 5, the reader is referred to the recent study of Ma et al. [9]. For detailed numerical and experimental for simpler axisymmetric problems, the work described in Lee [10] is applicable, particularly in “Chapter 3: Laboratory Experiments to Simulate the Downhole Environment of Mud-filtrate Invasion for Formation-Testing.”

Figure 4 COSL laboratory facilities and automated test controls.

Figure 5 Large-size core sample emphasis - different rock types shown.

2. Modeling Hierarchies Explained

Azimuthal formation tester hardware design and conceptual analysis was guided by new Darcy flow simulators, accounting for three-dimensional cylindrical borehole radius effects and close probe interactions. These do not use single point source approximations. Importantly, our models are designed for fully transient operations, and further, support overbalanced and underbalanced operations - for example, effects like time-dependent supercharge and local borehole invasion. On the other hand, axial tools may be modeled more simply using ideal source approaches, although numerical difficulties remained until very recently. Here we give simple explanations for the contrasting underlying assumptions. By "hierarchies," we refer to the most fundamental physical ideas first, as in Figure 6 and Figure 7 below, and later to those having greater implementation details.

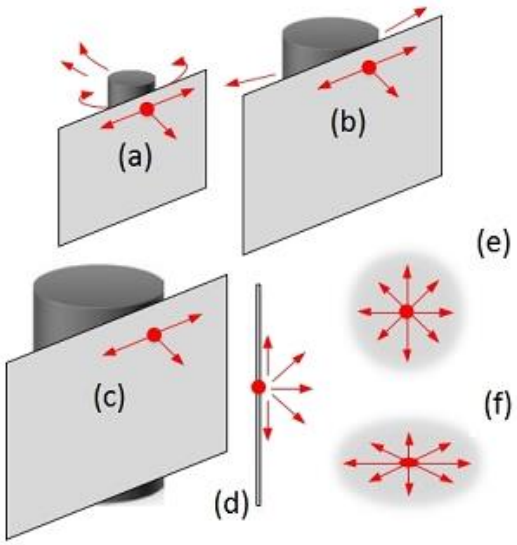

Figure 6 Source flow modeling hierarchies for axial sensor arrays.

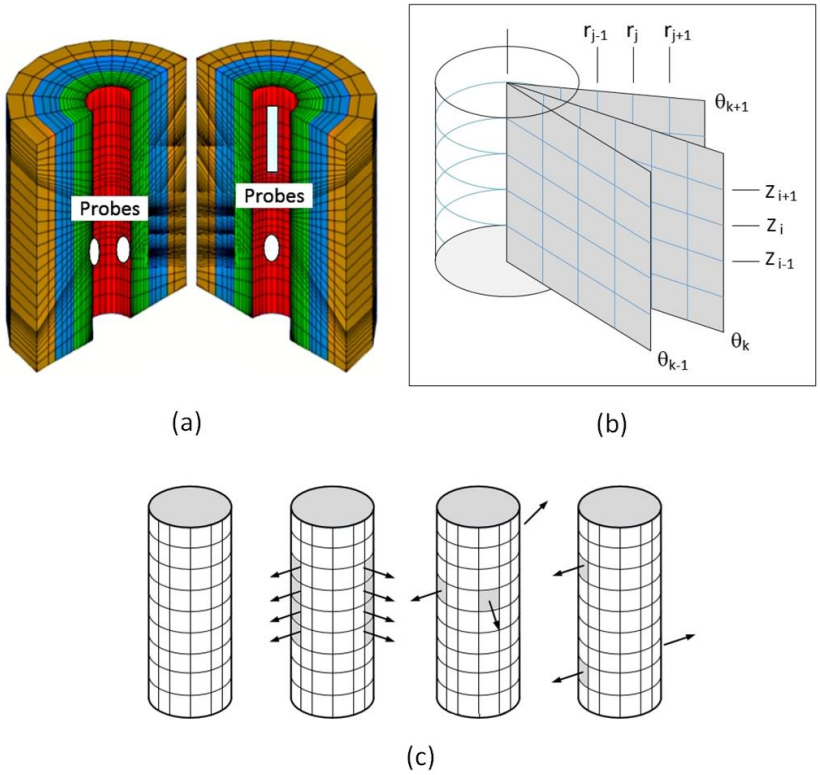

Figure 7 Three-dimensional mesh description, (a) circular polar coordinate grid system for vertical wells; (b) vertical z(i), radial r(j) and azimuthal θ(k) variables, where i, j and k are indexes, and (c) simulation shape implementation for slotted and round probe shapes.

2.1 Azimuthal Tool Models

We emphasize that idealized single source descriptions (used later, in our discussion of axial models) represent crude farfield methods that do not model nearfield azimuthal probe details. In reservoir flow analysis, long vertical wells are modeled with ideal line sources and narrow cylinders - this is justified, again in reservoir simulation, because circular constant pressure contours are always found a short radius away despite the presence of near-well irregularities. However, in modeling azimuthal formation testers like those in Figure 1, single source models alone are never applicable. All three sources must be modeled since complicated flow interactions, given the possibility of differences in flow rate profile, start and stop times, must be considered. The complete flow geometry must be studied, considering how individual nozzles may operate independently. This requirement means that a full geometry transient numerical approach accounting for inter-probe interactions and all fluid flow details is needed.

2.2 Axial Tool Models

Different scales for flow modeling are possible for individual probe nozzles. In Figure 6a, fluid emerges from the circular cylinder representing the well and into the reservoir. For now, a well impermeable to invasion is assumed to model an established mudcake. Streamlines oriented in all directions are shown, which ultimately turn around the borehole and into the page. As well radii increase, this turning effect is reduced, noticeably starting with Figure 6b. In Figures 6c and 6d, the

flat surface morphs into a symmetry plane separating dual portions of a reservoir that behave independently and identically. In this limit, the idea of the "ideal spherical and ellipsoidal source" in Figures 6e and 6f for isotropic and transversely isotropic formations emerges. We emphasize that these ideas apply to conventional formation testers with isolated probes and not multiple-probe tools with pressure gauges distributed about the well. The mathematics simplify considerably in describing the axial models of this section. The models in Chin et al. [1] can used to model axial formation tester flows for Figure 2 and Figure 3. Because wellbore radius and nozzle geometry effects, while small, nonetheless exist, a simple approach is used to correct for the lack of symmetry shown in Figure 6d. The geometric spherical or ellipsoidal nozzle radius Rnozzle is replaced by GRnozzle where the positive multiplicative constant "G" is found empirically from field or laboratory work, or by detailed computational analysis. "G" is commonly referred to as the "geometric factor."

Why use axial tool models? While triple-probe tools appear to offer greater information, at least at a fixed axial location, detailed axial measurements offer geological details in directions along the tool axis, related to layer boundaries and thicknesses, pressure gradient (fluid identification analysis), and axial resolution/depth of investigation information in array implementations. For the latter, as suggested in Figure 2, high integrity discernible pulses are necessary over large distances, given the highly diffusive, dispersive and attenuative formation environment. It no longer suffices to perform just single-probe pressure transient studies for the purposes of single-point properties prediction. It is imperative to employ high definition source pulses that can be tracked accurately as they propagate. An example of such a study is given in the "pressure versus time" versus probe location plots of Section 4.4.

Aside from the advantages described above, multiple axially separated observation probes offer detailed assessments on anisotropy important to wellbore stability, hydraulic fracturing and infill drilling. Single probe formation testers, drawing upon real-time algorithms like Halliburton's GeoTap™ invented by the last author in Proett, Chin and Chen [11], can at most predict the effective permeability $k_h^{2/3}k_v^{1/3}$. In weakly anisotropic media, this effective average is useful. However, when k_h and k_v differ significantly, as in many formations, this lumped quantity is lacking in anisotropic detail. Petroleum engineers require individual estimates for k_h and k_v for many reservoir development applications.

When a "dual probe tool" is used, consisting of one sink and one observation probe located some axial distance apart, it can be shown that independent values for k_h and k_v can be obtained. Four different methods are developed in Chin et al. [1]. These are summarized in this article in Section 4.1, "Why anisotropy modeling is important." Multiple dual probe combinations can be constructed, for example, from the array formation tester in Figure 2, allowing different axial resolutions at different depths of investigation to be studied. An important capability needed for such assessments is one which accurately predicts waveform attenuation, and diffusive and dispersive distortions as they depend on space, as will be discussed later in this paper. As with acoustic and resistivity logging tools, the integrity of the source signal is paramount.

Of course, k_h and k_v determination at a given axial location is also possible using azimuthal transducer arrays, such as that found in the triple-probe tool of Figure 1. Inverse methods have been developed for three and four probe arrangements and will be reported in Chin [6], a comprehensive 2024 book dealing with single and multiphase multiprobe dynamics in liquid and gas media. Interested readers may obtain pre-print copies from the last author.

3. Transient Three-Dimensional Azimuthal Model

Fully transient 3D computational fluid-dynamic "CFD" models are needed for pressure analyses if borehole radii and time-dependent different flow rates at multiprobe nozzles must be studied. Chin and Proett [12] attempted to account for such effects early on. In that study, an axisymmetric description was used, with the formation tester represented by a "ring" source. A model coupling transient pressure and contamination formulations for the two-phase flow was then solved using a finite difference method which was rapid and stable. Computational results in space, strictly applying to straddle packers, were displayed as "pressure and oil concentration snapshots" provided at different times. In the present analysis, axisymmetric assumptions do not apply and full three-dimensionality with azimuthal angular dependence is necessary.

In numerical modeling, different approaches are possible, the most popular being finite difference and finite element methods. The latter are known to provide geometric flexibility; for example, nozzle pad shape details are best modeled with finite elements. Finite difference methods are often used when key geometric features can be adequately described by standard host coordinate systems. This is our case, as shown in Figures 7a, 7b and 7c, in which a conventional cylindrical coordinate system readily accommodates all of the relevant boundary conditions described later. Another reason was practicality. The axisymmetric scheme of Chin and Proett [12] described above, also using finite differences, could be easily extended to three dimensions using well known methods in approximate factorization. The 2005 scheme was extended to include an angular dependence, plus additional stabilizing terms that would enable larger integration time steps for more rapid runs. Finally, we emphasize the limits in formation testing numerical modeling in many software simulators. At low permeabilities, the range 0.1-1.0 md is commonly successfully dealt with; however, permeabilities below 0.1 md describe "unconventional" reservoirs and applications which, to our knowledge, are seldom addressed (these values assume a fluid viscosity of 1 cp). On the other hand, high permeabilities, say 1,000 md or greater, may present problems in that pressures equilibrate so rapidly that the physics of the problem cannot be resolved on the time grids typically used. Of course, rapid pressure equilibration is also observed in field practice, so this is not really a "problem" with simulators in general.

3.1 Simulator Overview

Our methodology permits full azimuthal dependency. We solve the complete multi-dimensional anisotropic liquid pressure diffusion equation $k_v P_{zz} + k_h (P_{xx} + P_{yy}) = \phi\mu c P_t$ subject to several boundary specifications. The equation is initially converted to the circular cylindrical form $k_v P_{zz} + k_h (P_{rr} + 1/r\ P_r + 1/r^2\ P_{\theta\theta}) = \phi\mu c P_t$ where it is finite differenced. As is well known, a complete solution requires the definition of realistic boundary and initial auxiliary conditions.

3.2 Computational Details

Four boundary conditions are applied. First, volume flow rate pumping rates and schedules, together with flowline volume expansion terms, are applied at all source locations. Second, borehole sandface conditions are invoked, e.g., impermeable walls in the case of "no invasion," or in the event of invasion and supercharge, an appropriate overbalanced flow model

(underbalanced effects are also considered by modifying this condition). Third, periodicity conditions are used to convert an opened rectangular computational domain into a closed annular one. These three conditions, requiring additional explanation, are sketched in diagrams below and also shown in clearly boxed diagrams in Figures 8a, 8b, 8c and 8d. And fourth, regularity conditions calling for zero disturbance flow at infinity are used. Finally, since the problem is transient, an initial condition is also needed, that is, zero pressure disturbances at t = 0 for initially quiescent conditions. This completes the azimuthal probe description. The algorithm, which is unconditionally stable for wide ranges of input mobilities, generalizes the axisymmetric work of Chin and Proett [12]. For medium density variable meshes, such as that suggested in Figure 7a, fifteen seconds of computing time per simulation are required for Windows i5 computers.

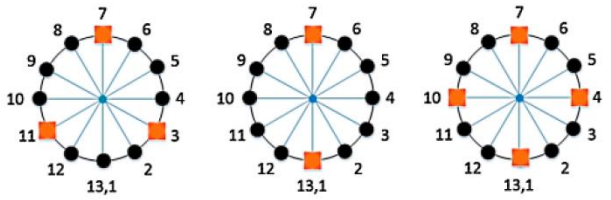

(a) Azimuthal node layouts, at left, index "7" denotes the main pumping probe, with "3" and "11" being 120° side probes, while "7" and "1," and "7," "4," "1," and "10" are other multiprobe possibilities (overlapping "1" and "13" are auxiliary overlapping indexes used to enforce periodicity constraints).

Let $\partial P/\partial r \approx (P_2 - P_1)/\Delta r$, so that $P_1 = P_2 - Q\mu\Delta r/(Ak_h) - \{\mu\Delta r/(Ak_h)\}(VC\partial P/\partial t)$. In coding, set $P_\Delta = Q\mu\Delta r/(Ak_h)$ and *Coef* = $VC\mu\Delta r/(Ak_h)$, so that backward differences at time level "n" yield $P_1^n = P_2^n - P_\Delta - Coef\ (P_1^n - P_1^{n-1})/\Delta t$. Regrouping, $P_1^n = (P_2^n - P_\Delta - Coef\ P_1^{n-1}/\Delta t)/(1 + Coef\ /\Delta t)$ which is unconditionally stable. Model applies to single and linear arrangements of panels for "small round and long slot" nozzles. Geometrical factors used as necessary from calibrating data obtained experimentally in test fixtures as in Figures 4 and 5. Fluid compressibility appears in two places, "c" in differential equation and "C" in boundary condition for pumping interactions. Software switch toggles code between round and long nozzle geometric options.

(b) Flowline volume simulation algorithm.

If mudcake completely seals rock, impermeable flow requires $P_1 = P_2$, relating pressures at nodes j = 1 and 2. If mud filtrate invasion is ongoing, well P_{mud} affects pressure in formation. Connect P_1, P_2 and P_{mud} by matching Darcy velocities, $(k_c/\mu_f)/(P_{mud} - P_1)/x_c(t) = (k_h/\mu)\ (P_1 - P_2)/\Delta r$, where k_c is cake permeability, μ_f is filtrate viscosity and $x_c(t)$ is cake thickness that varies with time. General models for dynamically coupled mudcake growth in multiphase flow appear in Chin and Proett (2005) and Chin et al. (2014). Dimensionless cake and filtration constants introduced with field procedures to determine their values. Here we assume $\mu_f = \mu$ and $x_c(t)$ is a prescribed constant. Foregoing solved to give $P_1 = (P_2 + D\ P_{mud})/(1 + D)$ where dimensionless $D = k_c\ \Delta r/(k_h\ x_c)$ controls physics. If it vanishes, impermeable wall conditions apply at sandface; if infinite, implying mudcake much more permeable than formation, sandface and mud pressures are identical. Model also applies to underbalanced drilling, in which case we might assume, e.g., zero pore pressure and negative mud pressure.

(c) Borehole wall boundary condition model.

In Figure 8a, we take θ_o as position "1," coincident with bottom node "13." We consider first-order accuracy. The forward first derivative is $P_1' = (P_2 - P_1)/\Delta\Theta$ while the backward value is $P_{13}' = (P_{13} - P_{12})/\Delta\Theta$. Set the two equal implies $P_2 - P_1 = P_{13} - P_{12}$. Since $P_1 = P_{13}$, we find that $P_1 = P_{13} = (P_2 + P_{12})/2$. Thus the pressures at "1" (or "13) are the arithmetic average of the values P_2 and P_{12}. This relation is used along all θ values at "1" or "13." Next consider second-order accuracy in ΔΘ. Backward and forward results yield $P_{13}' = (3P_{13} - 4P_{12} + P_{11})/(2\Delta\Theta)$ and $P_1' = (-P_3 + 4P_2 - 3P_1)/(2\ \Delta\Theta)$. Setting the two equal yields $3P_{13} - 4P_{12} + P_{11} = -P_3 + 4P_2 - 3P_1$ or, on denoting $P_{temp} = P_1 = P_{13}$, the relation 6 $P_{temp} = 4P_2 + 4P_{12} - P_3 - P_{11}$. Finally, $P_1 = P_{13} = (2/3)\ (P_2 + P_{12}) - (1/6)\ (P_3 + P_{11})$. This contains the correct symmetries, with an $O(\Delta\Theta^2)$ error formally smaller than that for $P_1 = P_{13} = (P_2 + P_{12})/2$, but the simpler first-order relation provides better accuracy. This is so since the pressures in "(1/6) $(P_3 + P_{11})$," in fact, reside at the 120° locations which where strong pump rates may exist, thus leading to large truncation errors. Numerical tests indicate that the simpler approach introduces at most 1% errors.

(d) Algorithm for periodicity conditions modeling.

Figure 8 Multiprobe boundary condition solution strategy.

Again, the overall approach is conceptualized in Figures 7a, 7b and 7c. These sketches are qualitative, and to implement the numerical objectives stated, details related to the finite differencing scheme will be discussed. In our work, we actually studied several families of commercial multiprobe tools. These are suggested in Figure 8a, where the left diagram, showing three (red square) source probes, represents the triple-probe tool discussed in this paper. The middle and right diagrams represent Schlumberger MDT™, Saturn™ and ORA™ multiprobe formation testers. Results of our comparisons are forthcoming in Chin [6]. Note that the ORA™

multiprobe formation tester, and certain Halliburton [7] and BakerHughes [8] concepts, may include several azimuthal multiprobe networks stationed at different axial positions.

The transient, anisotropic, three-dimensional pressure diffusion equation used is given by $k_v P_{zz} + k_h (P_{xx} + P_{yy}) = \phi\mu c P_t$. Here, k_v applies in a vertical z direction aligned with the tool's wireline axis, and k_h applies laterally in the x and y horizontal directions. Through standard "rectangular to polar coordinate transformations," we can re-express this as $k_v P_{zz} + k_h (P_{rr} + 1/r\ P_r + 1/r^2\ P_{\theta\theta}) = \phi\mu c P_t$ to accommodate circular well cross-sections. Here, P is pressure, r and θ are radial and polar coordinates, t is time, ϕ is porosity, μ is viscosity, and c is liquid compressibility. The foregoing equation is solved with uniform initial and farfield conditions, however, during the simulations, sandface pressure values may change due to nozzle pumping and borehole invasion. Note that the value of "ϕμc/k" can be chosen to accelerate computing speed if we only require steady-state solutions. This is useful in "batch processing" to generate large data volumes for use in steady-state history matching or "big data" machine learning algorithms. Boundary conditions are discussed next.

3.3 Flowline Volume Storage Modeling

For the tools in Figures 7 and 8a, flow rate specifications are written as $A(k_h/\mu)\ \partial P/\partial r = Q$ using Darcy's equation. Here A is the curved panel area $R\Delta\Theta dz$, μ is a Newtonian viscosity, k_h is the horizontal permeability for flow normal to the panel, Q is volume flow rate, and "r" is the radial variable. This is the conventional rate model used in reservoir engineering connecting k_h to other quantities. When flowline volumes V are dynamically important, with this being especially so at low mobilities, we must consider the more complete $A(k_h/\mu)\ \partial P/\partial r = Q + VC\ \partial P/\partial t$ or $\partial P/\partial r = \mu/(Ak_h)\ [Q + VC\ \partial P/\partial t]$ explained in the book by Lu et al. [5] where C is the flowline liquid compressibility. The finite difference equations used to model flowline volume effects is succinctly described above in Figure 8b.

3.4 Active Flowline Volume Coupling at Observation Probes

"Observation probes" are probes that ideally play passive non-pumping roles in formation testing. However, engineers have found that these may react to pumping at the pumping probe. In other words, hydraulic interactions between pumping and observation probes exist. This communication is known as "active flowline coupling." When pumping is absent, that is $P_\Delta = 0$, we implement $P_1^n = (P_2^n - \mathit{Coef}\ P_1^{n-1} / \Delta t) / (1 + \mathit{Coef} / \Delta t)$ instead, which includes volume changes due to flowline compressibility. The coupling is small and vanishes as V decreases.

3.5 Borehole Invasion, Pressure Supercharging, Plus Underbalanced Effects

In general, the borehole sandface is not impermeable to flow. High pressures in the well may lead to invasion and high "supercharge" pressures. On the other hand, high reservoir pressures may cause fluid loss into the well and result in underbalanced pressures. These events affect the pressures measured at formation tester nozzles. If wellbore effects are significant, the pressures measured by the tool cannot be directly used for inverse permeability prediction unless they are appropriately corrected. Otherwise, errors in predicted properties appear. We also emphasize that the supercharge model in this paper and in Chin [6] describes the complete process beginning with

mudcake buildup, whereas Lu et al. [4] starts with a spatially varying initial pressure condition resulting from invasion prior to formation tester pumping from an idealized point source.

3.6 Modeling Periodicity in Annular Domains Wells

If $P(\theta)$ is periodic in θ starting at a $\theta = \theta_o$, and it and its derivatives are continuous with $P^+(\theta_o) = P^-(\theta_o)$ and $\partial P^+(\theta_o) / \partial\theta = \partial P^-(\theta_o) / \partial\theta$, numerical implementation is straightforward with finite differences. Two methods are summarized in Figure 8d.

Figure 9 shows a rectangular block "morphing" to accommodate annular constraints when left and right ends are joined. Finally, we offer descriptions of tool and probe orientations used in our modeling in Figure 10 and Figure 11. The present section deals with azimuthal probes. Note that multiple axial probes can be added to the above software for the tools in Figures 1a and 1b by simply duplicating source code blocks developed from the math model in Section 4. Finally, the partial differential equation for pressure can be differenced using "approximate factorization" or "alternating direction implicit" (ADI) methods and integrated in time, subject to the auxiliary conditions derived in Figures 8b, 8c and 8d.

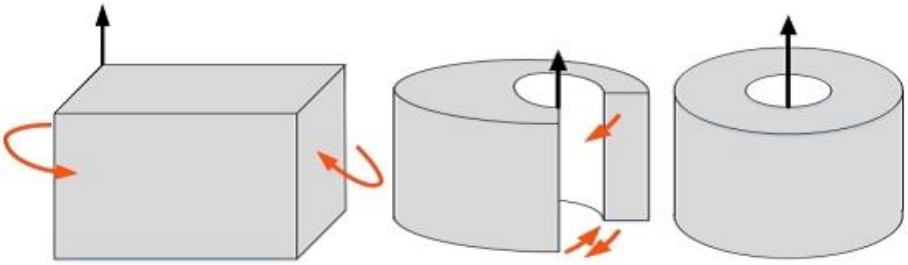

Figure 9 Periodicity requires special matching constraints.

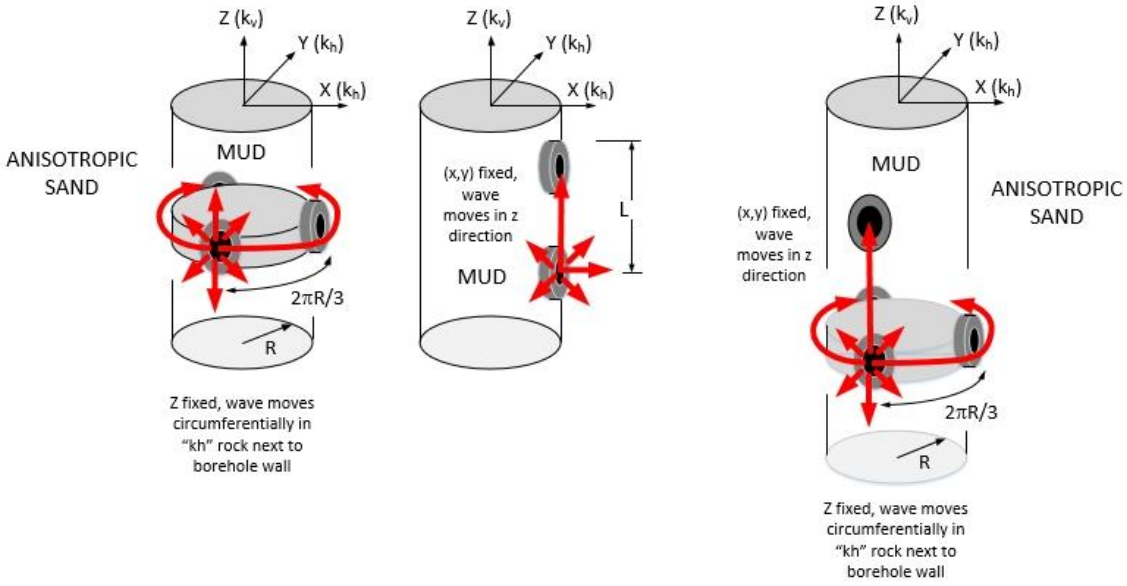

Figure 10 Tool configurations supported by present algorithms.

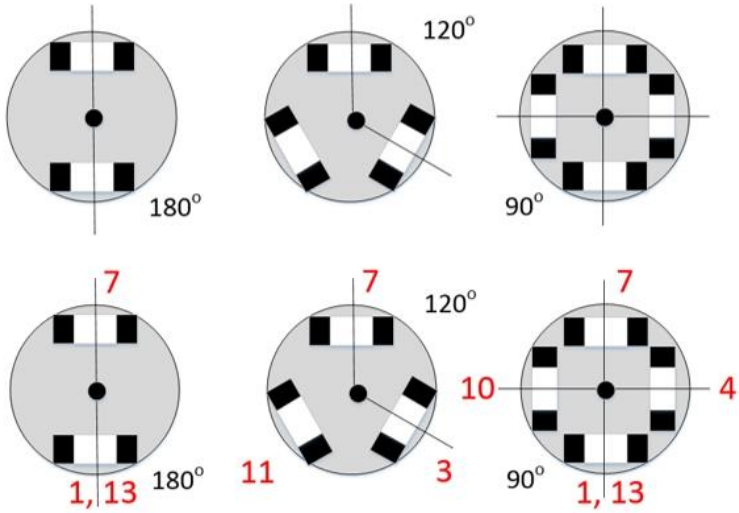

Figure 11 Probe position numbers for triple-probe tools.

3.7 Applications of Azimuthally Distributed Formation Testing Probes

Extensive details describing the new "three arm" formation testing tool, as well as the results of an extensive suite of validation and applications examples, are forthcoming in book publication [6]. In this paper, we highlight seven non-trivial simulations which demonstrate our capabilities in modeling fluid influx and outflux in overbalanced and underbalanced drilling. For brevity, our calculations will be restricted to Schlumberger MDT™ type round nozzle applications with an active sink Probe 7 and a passive observation Probe 1. Pressure responses at 120 deg positions "3" and "11" are also given to demonstrate attenuations calculated in the circumferential direction. As noted, this article focuses on single-phase applications, particularly for triple-probe tools. A comprehensive volume dealing with general three and four nozzle multiprobe tools operating in single and multiphase environments is scheduled for 2024 publication in Chin [6], describing coupled pressure and miscible contamination issues, in addition to inverse solutions, high-speed batch solutions and convergence acceleration methods.

3.7.1 Example 1 Drawdown with Round Nozzle, Plus Invasion with 200 Psi Overbalance

We consider formation testing in overbalanced drilling and select "Invasion, supercharge" in Figure 12a. This selection leads to a second menu asking for the overbalance pressure and a dimensionless "cake to rock mobility" ratio. We selected a convenient zero pore pressure for reference and a mud overbalance of 200 psi. The latter ratio measures mudcake permeability relative to that of the formation. If it is zero, we have an impermeable cake with a sealed sandface. If positive, the sandface supports invasion. Invasion and contamination depend on cake filtration properties measurable using filtration presses. If not, more detailed flow characterization is required. Methods and issues are described in Chin et al. [1] relating measured data to the mobility ratio from Figure 12a.

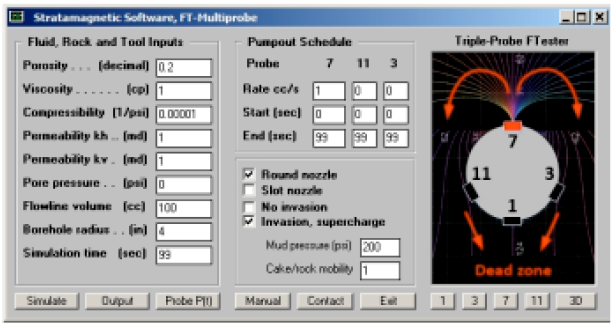

(a) Invasion and supercharge example.

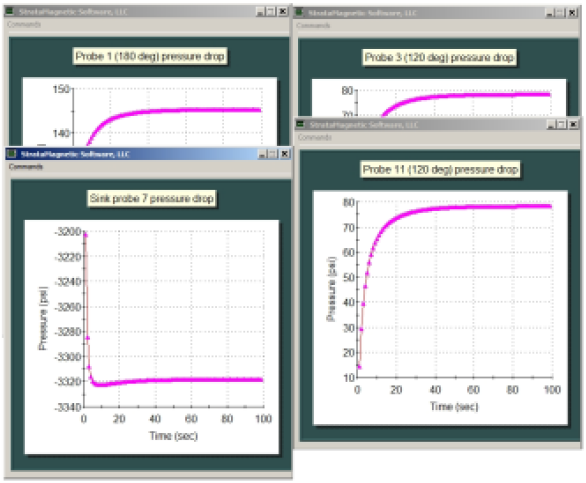

(b) Unsteady behavior at Probes 1, 3, 7 and 11.

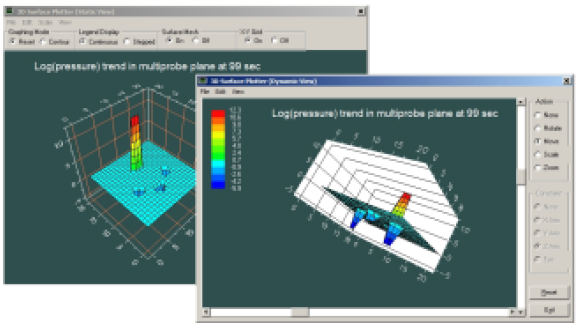

(c) Logarithmic display for Probes 1, 3, 7 and 11 (different pressure signs found for probes due to supercharge).

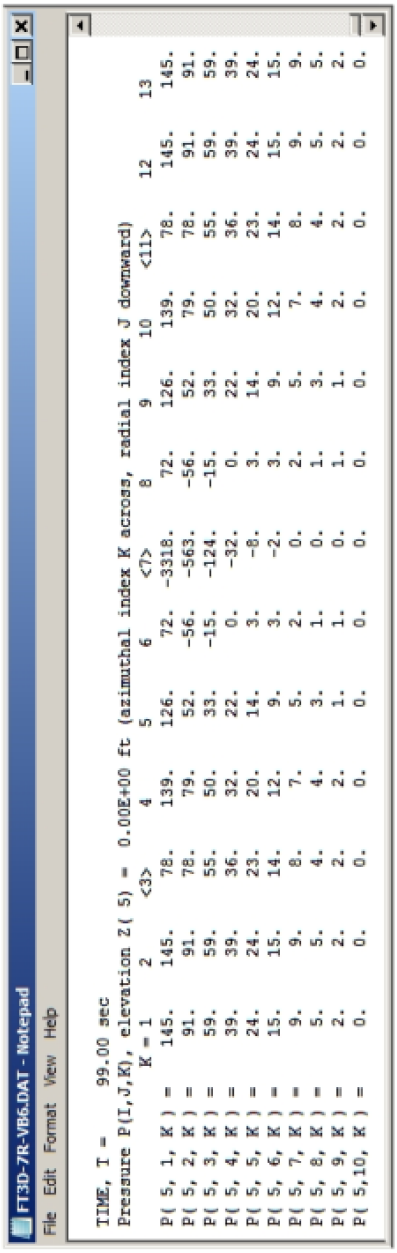

(d) Pressures in a plane normal to borehole centerline passing through sink, with azimuthal versus radial position.

Figure 12 Supercharge calculation with 200 psi overbalance pressure.

Transient pressures at Probes 1, 3, 7 and 11 appear in Figures 12b and 12c. The line for sink Probe 7 displays the expected pressure decline. After an initial sudden drop, a slow increase is found. Time-wise pressure increases are seen at Probes 1, 3 and 11. These are due to filtrate invasion from the borehole. Finally, we give the tabulation in Figure 12d for pressures along the sandface circumference J = 1 and that along the circle at J = 2 just one radial grid block away. The difference in pressure (at any given K, away from the sink probe) describes the imbalance contributing to slow invasion. The much larger difference at K = 7 measures the significant differential due to pumping. Our model supports both over and underbalanced drilling.

3.7.2 Example 2 Drawdown with Round Nozzle, Invasion with 2,000 Psi Overbalance

The 200 psi excess pressure in Example 1 is commonly cited in the older literature. Such values severely underestimate actual conditions. Recent estimates using formation tester measurements are much more severe. Two major exploration companies describe their field observations in surveying numerous wells in Southeast Asia. Rourke et al. [13] cite Halliburton and Chevron measurements in their paper "A New Hostile Environment Wireline Formation Testing Tool: A Case Study from the Gulf of Thailand," and summarize field observations from over *three hundred* wells logged with a new formation tester. In short, "While pressure testing in the infill development wells where depletion is often observed, it is not uncommon for the differential between hydrostatic and reservoir pressure to exceed 2,000 psi." This is reiterated a decade later in a 2018 posting [14] entitled "Testing the Tight Gas Reservoir - Hostile Environment Wireline Formation Tester Reduces NPT in HPHT Boreholes," available at www.halliburton.com. "Wells are drilled highly overbalanced because the differential between hydrostatic and reservoir pressure may exceed 2,000 psi."

Here, we repeat Example 1, assuming 2,000 psi instead of 200 psi. Our assumptions and calculated results are given in Figures 13a, 13b, 13c and 13d. Note how, in Figure 12b for sink Probe 7 at the bottom left, the pressure transient curve sharply decreases in time and then rises slightly (the pressures at Probes 1, 3 and 11 always increase despite the 1 cc/s drawdown). The corresponding pressure curve at Probe 7 in Figure 13b always increases, a direct consequence of strong overbalance pressure effects.

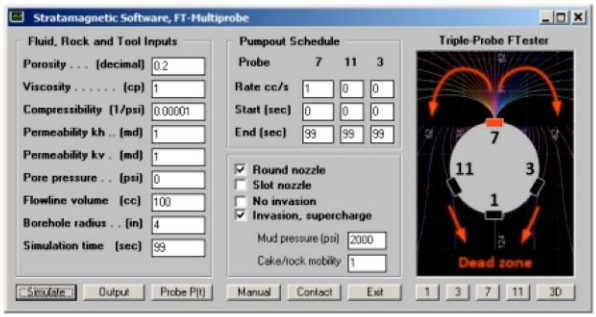

(a) High supercharge input variables.

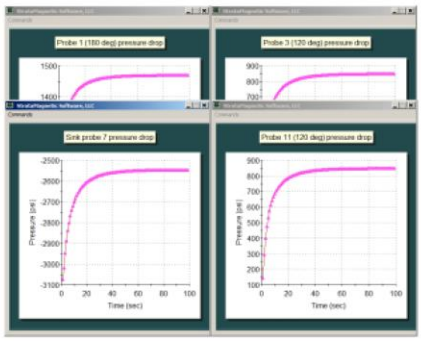

(b) Very high supercharge pressure transient responses – note how pressures increase at Probe 7 despite fluid withdrawal (this is attributed to very strong overbalance).

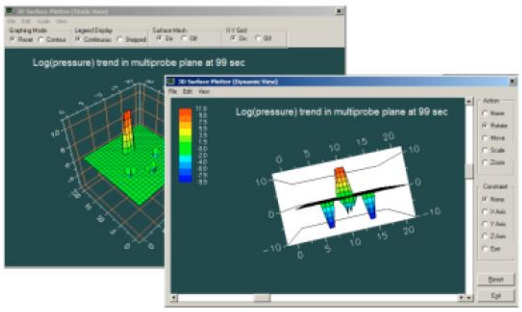

(c) Logarithmic pressure probe responses clearly demonstrate the physics.

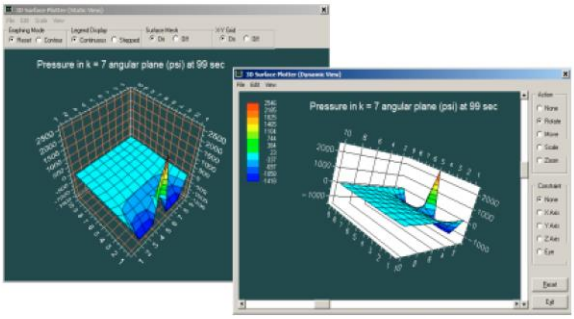

(d) Transient results at azimuthal sink plane, t = 99 sec.

Figure 13 Supercharge calculation with 2,000 psi overbalance pressure.

3.7.3 Example 3 Drawdown with Round Nozzle, Assuming 100 Psi Underbalance

Keeping reservoir pressures above borehole levels supports increased drilling penetration rates and reduces formation damage. While our methodology emphasizes overbalanced applications, the same problem formulation permits reservoir pressures to exceed those in the well, that is, underbalanced drilling, in which case fluid exits the reservoir and into the well through the sandface (in this application, there is no mudcake). Needed input changes are given in Figure 14a, while calculated results are displayed in Figures 14b and 14c.

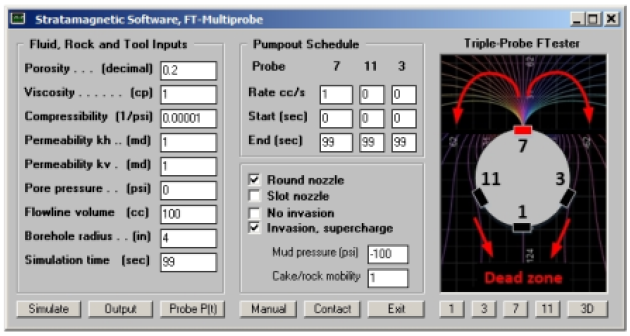

(a) Underbalanced pressure with "– 100 psi" relative to "0" pore pressure.

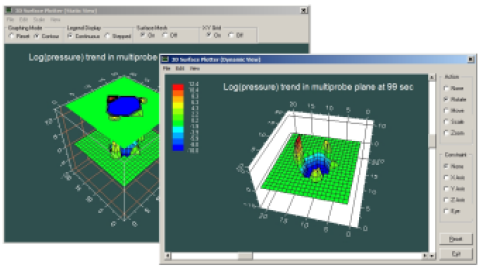

(b) Pressure response at t = 99 sec.

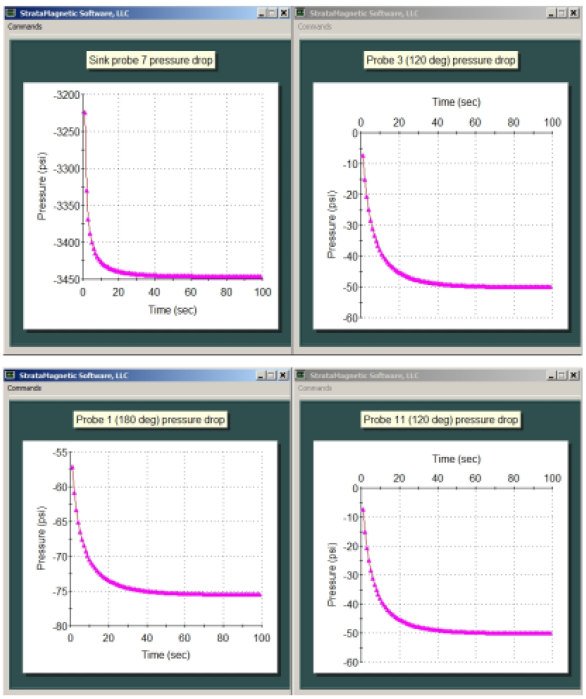

(c) Pressure drawdown time histories.

Figure 14 Calculations for underbalanced drilling.

3.7.4 Example 4 Drawdown with Three Pumping Slot Nozzles and No Invasion

Next consider a full triple-probe formation tester configuration with 120° angular separations. The probes simultaneously withdraw fluid at the same rate over identical time periods. Figure 15 below summarizes all simulation details. The model inputs used are given in Figure 15a, while computed results are displayed in Figures 15b, 15c, 15d, 15e, 15f and 15g.

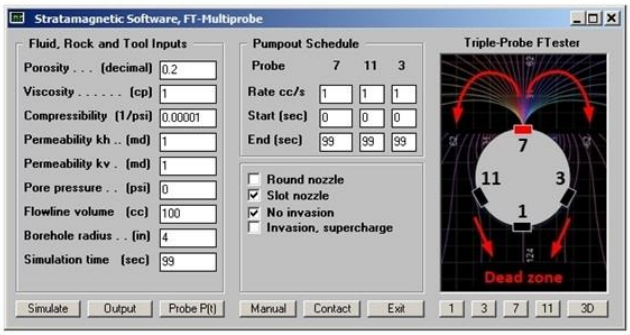

(a) Triple-slot nozzles pumping at identical rates.

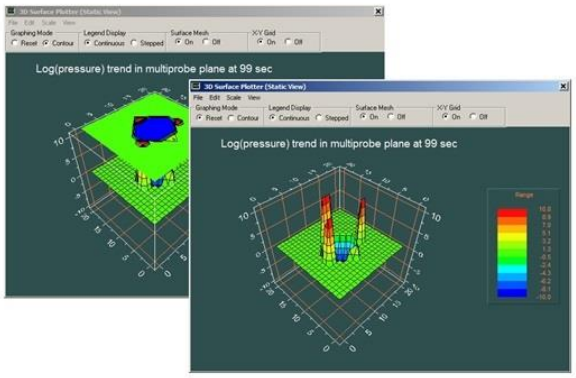

(b) Logarithmic pressure field using static display feature.

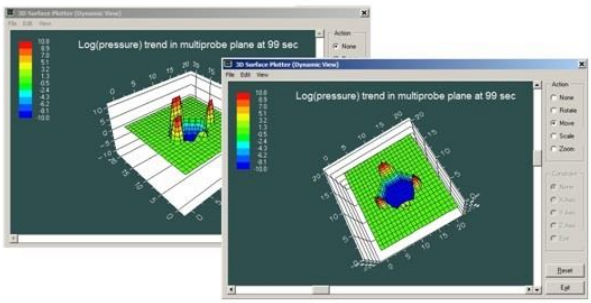

(c) Logarithmic pressures using mouse-rotatable dynamic display.

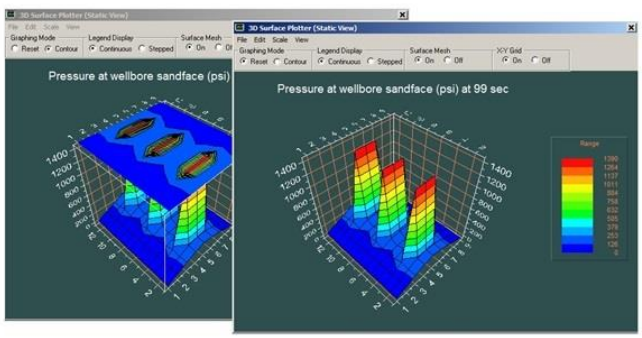

(d) Triple-probe slot pressures "unwrapped" in sandface plane.

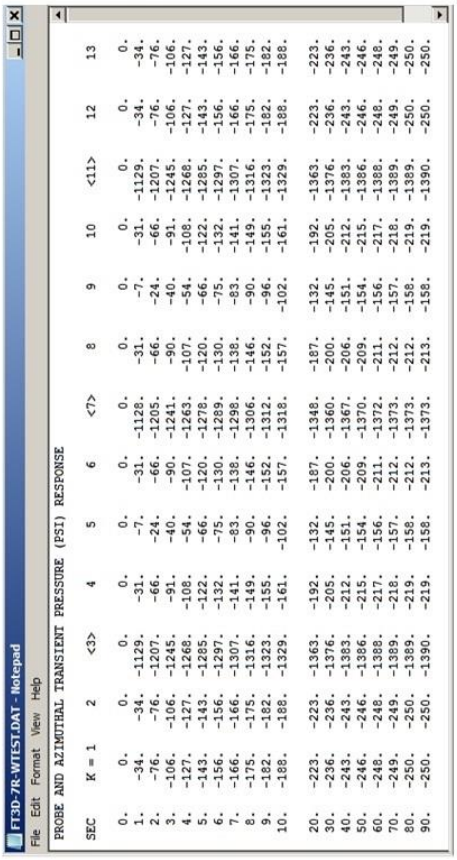

(e) Pressures at all angles (symmetry obtained about K = 7 position).

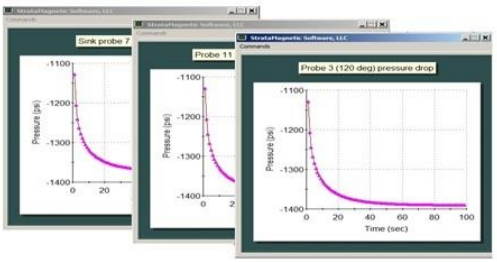

(f) Almost identical responses despite approximate periodicity conditions.

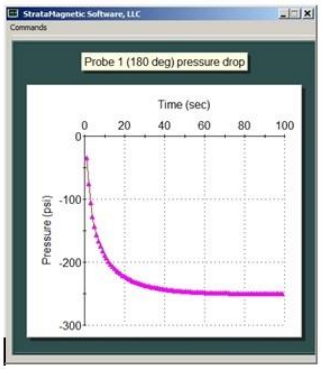

(g) Computed pressure at *passive* midway observation probe.

Figure 15 Drawdown with Three Pumping Slot Nozzles and No Invasion.

Figure 15d displays “line pressure” traces anticipated for the three slot nozzles conveniently plotted over an “unwrapped” sandface. The right-side perspective view shows how the 120° pressure distributions are identical. We also investigated more closely numerical accuracy details. Figure 15e tabulates pressure values at all angular positions, noting that probe indexes are K = 3, 7 and 11. At 1 sec, we calculated 1,129, 1,128 and 1,129 psi respectively, while at 90 sec, these become 1,390, 1,373 and 1,390 psi. The difference between largest and smallest values arises because physical symmetries are compromised by branch cut logic that enforces periodicity conditions. However, the differences are only about 1%.

The difference is not perceptible even in the close-up view of Figure 15f, which omits the significant decline between t = 0 and 1,100 sec. Again the minor difference, arising from the implementation of periodicity conditions, can be readily remedied by selecting small adjustments to individual geometric factors. Note how the passive observation probe at the 180° location experiences a 250 psi decline versus a 1,400 psi pressure drawdown.

3.7.5 Example 5 Three Round Nozzles, Simultaneous “Drawdown and Buildup” with Different Pump Rate Histories and No Invasion

Here we illustrate additional computational capabilities. Example 5 is summarized in Figures 16 and 17, in particular, in Frames (a), (b), (c), (d), (e) and (f). We examine on the central portion of Figure 16a. To withdraw fluid using all three nozzles, we enter (different) nonzero values into the required “Rate cc/s” box, followed by desired starting and ending times. Flow rates need not be identical - they may differ in sign, so that mixed injections, withdrawals or zeros are supported. We have checked “Round nozzle” and “No invasion.” Pumping all three probes provides full and true 360 deg coverage for heterogeneity and anisotropy mapping, not possible with single and dual probe tools such as those studied in [1], [2] and [3].

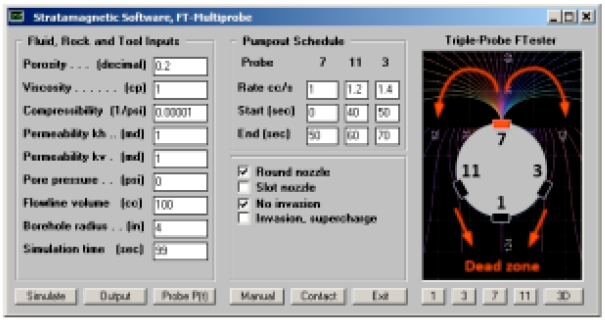

(a) Complex pumping schedule, different rates and times.

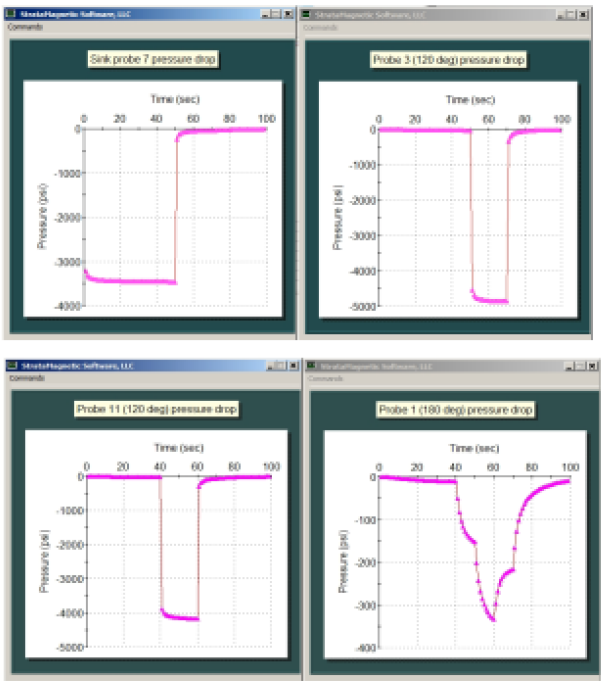

(b) Drawdown behavior at different probe positions.

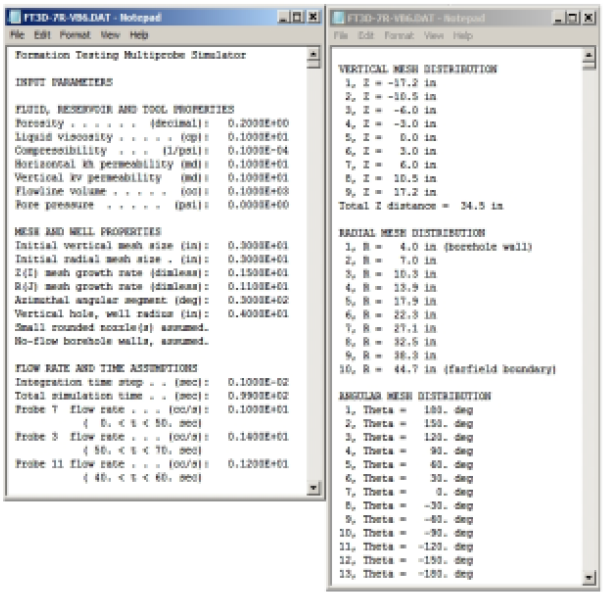

(c) Input summary from "Output" button.

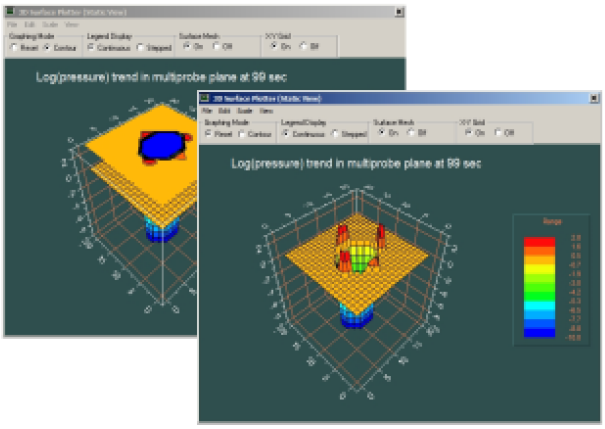

(d) Computed pressure responses at t = 99 sec.

Figure 16 Computational details (a), (b), (c) and (d) for Example 5.

This simulation, encompassing a range of complications, requires the same computing time and resources as the simplest run. The pressure curves in Figure 16b are produced within 15-20 sec. The histories for probes 3, 7 and 11 are consistent with the entries in Figure 16a as they are dominated by suction pressures (refer to the input summary in Figure 16c). The curve for non-pumping, passive observation Probe 1 at 180° is interesting, showing a complicated pattern of superpositions that would have been difficult to anticipate. Figures 16d and 17 provide additional calculated pressure behavior.

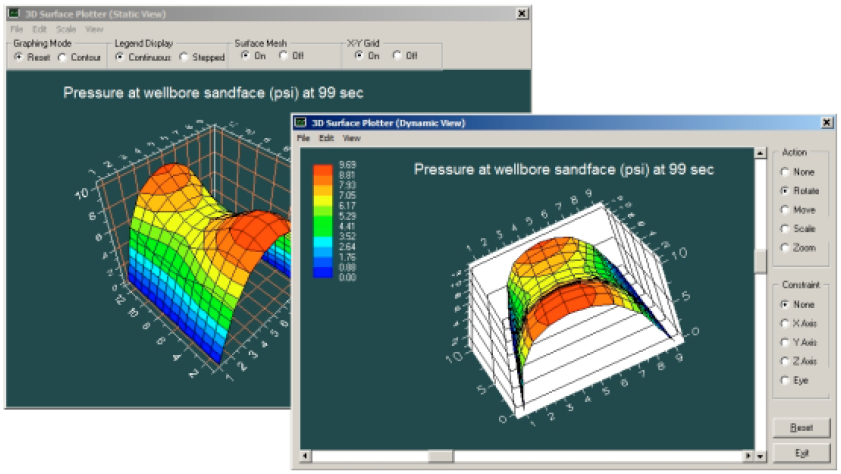

(e) Pressure displayed on "unwrapped" sandface.

FT3D-7R-WTEST.DAT - Notepad

File Edit Format View Help

PROBE AND AZIMUTHAL TRANSIENT PRESSURE (PSI) RESPONSE

SEC	K = 1	2	<3>	4	5	6	<7>	8	9	10	<11>	12	13
0.	0.	0.	0.	0.	0.	0.	0.	0.	0.	0.	0.	0.	0.
1.	0.	0.	0.	0.	-6.	-59.	-3218.	-59.	-6.	0.	0.	0.	0.
10.	-3.	-3.	-7.	-19.	-57.	-179.	-3426.	-179.	-57.	-19.	-7.	-3.	-3.
15.	-5.	-5.	-10.	-25.	-65.	-190.	-3438.	-190.	-65.	-25.	-10.	-5.	-5.
20.	-7.	-7.	-13.	-28.	-70.	-196.	-3444.	-196.	-70.	-28.	-13.	-7.	-7.
25.	-8.	-8.	-14.	-31.	-73.	-199.	-3448.	-199.	-73.	-31.	-14.	-8.	-8.
30.	-10.	-10.	-16.	-32.	-75.	-202.	-3451.	-202.	-75.	-32.	-16.	-10.	-10.
35.	-10.	-10.	-17.	-33.	-76.	-203.	-3452.	-203.	-76.	-33.	-17.	-10.	-10.
40.	-11.	-11.	-17.	-34.	-77.	-204.	-3453.	-204.	-77.	-34.	-108.	-11.	-11.
45.	-127.	-42.	-25.	-37.	-78.	-206.	-3457.	-217.	-126.	-220.	-4097.	-213.	-127.
50.	-153.	-57.	-140.	-41.	-81.	-209.	-3463.	-229.	-147.	-253.	-4137.	-249.	-153.
55.	-299.	-300.	-4796.	-250.	-99.	-73.	-74.	-83.	-118.	-259.	-4159.	-298.	-299.
60.	-334.	-345.	-4841.	-281.	-109.	-62.	-54.	-65.	-110.	-262.	-4173.	-323.	-334.
65.	-233.	-333.	-4851.	-292.	-114.	-60.	-46.	-48.	-60.	-79.	-101.	-133.	-233.
70.	-216.	-327.	-4852.	-295.	-116.	-59.	-39.	-36.	-40.	-49.	-66.	-104.	-216.
75.	-74.	-89.	-92.	-80.	-60.	-42.	-32.	-28.	-30.	-35.	-45.	-59.	-74.
80.	-41.	-46.	-47.	-43.	-35.	-28.	-23.	-21.	-22.	-25.	-30.	-36.	-41.
85.	-26.	-28.	-29.	-27.	-23.	-20.	-17.	-16.	-16.	-18.	-21.	-23.	-26.
90.	-17.	-19.	-19.	-18.	-16.	-14.	-12.	-12.	-12.	-13.	-14.	-16.	-17.
95.	-12.	-13.	-13.	-12.	-11.	-10.	-9.	-9.	-9.	-9.	-10.	-11.	-12.
99.	-9.	-10.	-10.	-9.	-9.	-8.	-7.	-7.	-7.	-7.	-8.	-9.	-9.

(f) Pressure transient values at all angular positions.

Figure 17 Computational details (e) and (f) for Example 5.

3.7.6 Example 6 Transient Flow Results for Mixed Round and Slot Nozzle Combinations with Different Pump Schedules (Impermeable Sandface)

This calculation shows how numerical stability is maintained for a problem where flow rates, starting times and nozzle types all vary substantially in a four nozzle multiprobe tool. The results reinforce our belief that the algorithm supports a broad variety of pumping actions for future unanticipated workflows. Inputs and outputs are summarized in Figure 18.

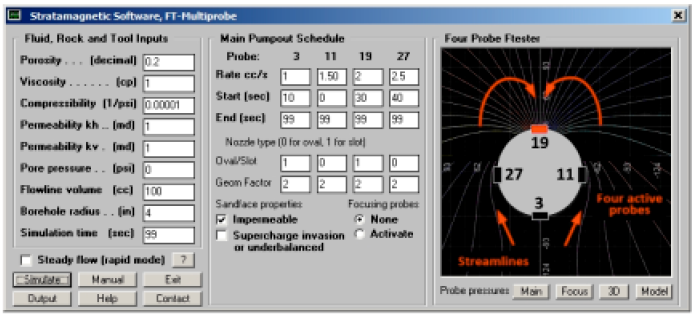

(a) A challenging run with "wildly" varying input data (note different menu used).

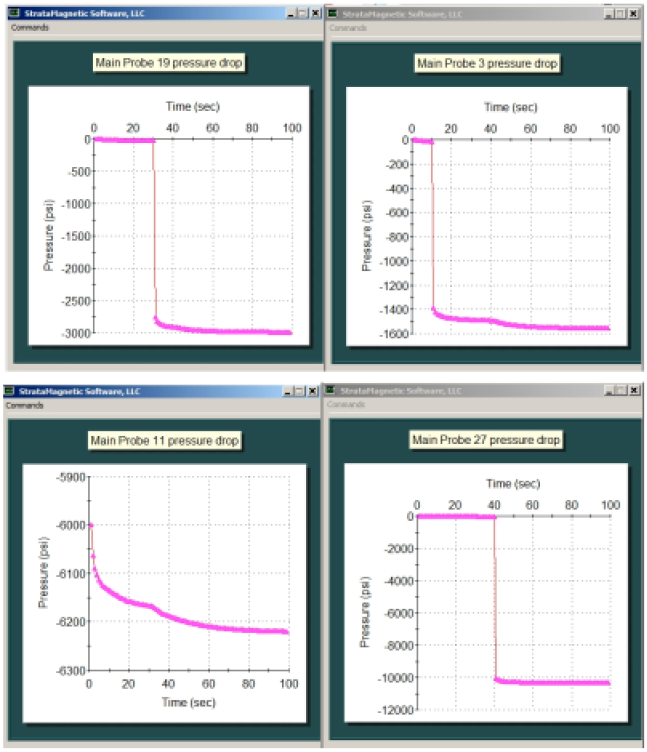

(b) Computed pressure responses in time.

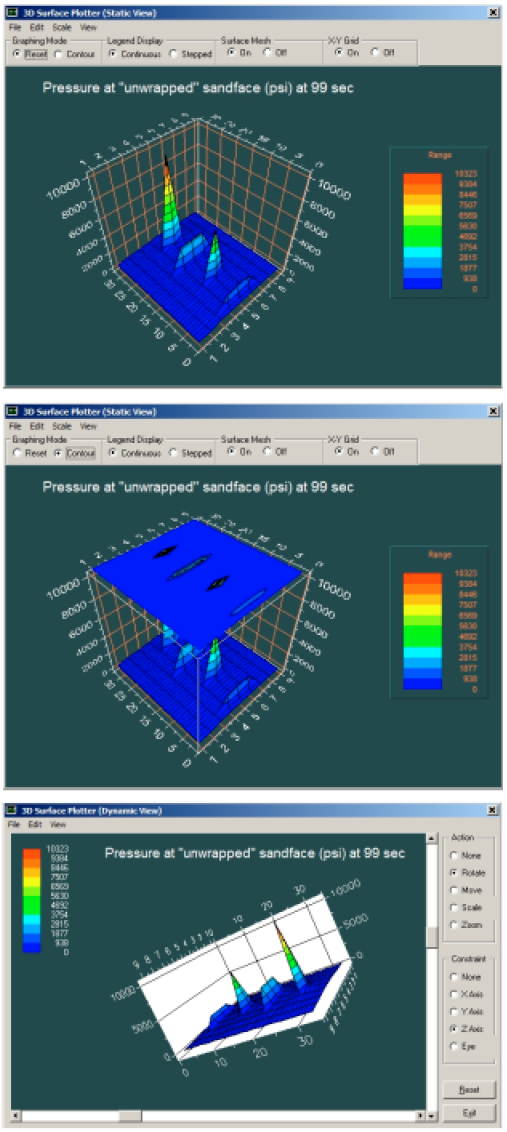

(c) Computed pressure responses in space.

Figure 18 A mixed nozzle, mixed flow rate calculation.

3.7.7 Example 7 Transient Flow Results for Mixed Withdrawal and Injection Flow Rates for Round and Slot Nozzle Combinations (Impermeable Sandface)

As indicated in the input menu in Figure 19a, we withdraw fluid at slot nozzles while injecting fluid at the same rate at "round" nozzles. The nozzle types alternate in geometry for the four-probe tool considered. We expect decreasing pressure at withdrawal sites and increasing pressure at injection sites. The magnitudes associated with smaller round nozzle areas should be higher than those for slot nozzles, about three times, approximately equal to the multiplicative change in nozzle area. The foregoing expectations are confirmed in calculations. This problem is not an academic exercise. In many field applications, chemicals are introduced into the formation to facilitate special treatments and progress is monitored by recording local pressures. Applications

include injections to increase local permeabilities and targeted heat delivery objectives. Calculated results appear in Figures 19b, 19c, 19d and 19e.

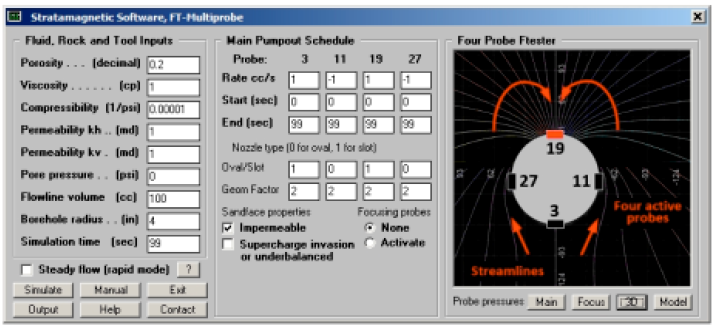

(a) Mixed withdrawal-injection rates with mixed nozzles (four probe tool).

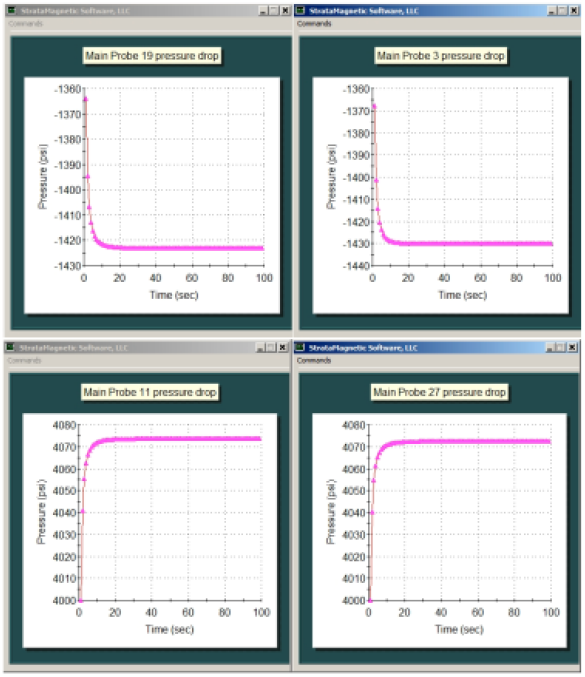

(b) Drawdown and buildup, consistent with flow rate type.

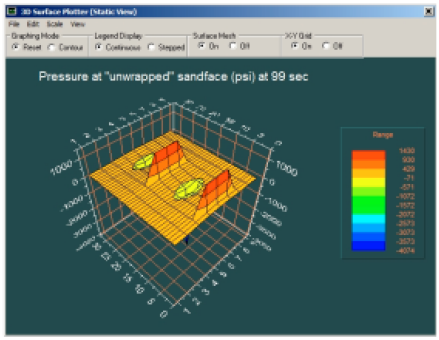

(c) 3D pressures, static plot.

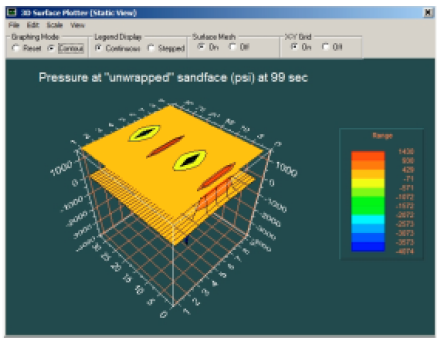

(d) 3D pressures, contour plot.

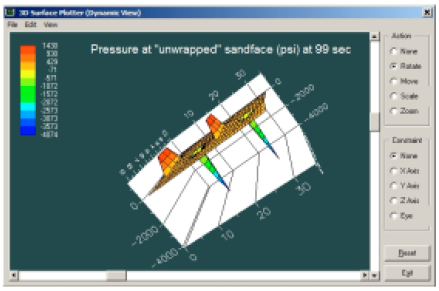

(e) 3D pressures, rotatable plot.

Figure 19 Mixed withdrawal and injection for mixed nozzle run.

4. Axial Multiprobe Tools - Array Design Considerations

In Examples 1-7, we studied azimuthal pressure probe responses and their dependence on probe number, nozzle shape, flow rate, rock properties, and start-stop times. The complete three-dimensional transient Darcy equation was modeled in vertical and cylindrical radial coordinates. In formation testing, circumferential nozzle arrays alone may not suffice. It is often desirable to add axial sensor arrays parallel to the tool axis, so that pressure data are available across multiple layers. Azimuthal and axial measurements together provide the data base needed for detailed heterogeneity, anisotropy and permeability characterization. This section focuses on properties prediction using axially distributed pressure transducers.

4.1 Why Anisotropy Modeling is Important

Single transducer formation testers, for example, that in Figure 2 with only the left-most element retained, can be used in elementary pressure transient analysis in various ways. For example, in situ fluid can be withdrawn from the rock, resulting in a pressure drawdown. Withdrawal and stoppage, on the other hand, lead to drawdown-buildup pressure behavior. Alternatively, injections used in chemical enhancement produce buildup and buildup-drawdown curves. Chin et at. [1] shows how compressibility and permeability can be predicted from any three "pressure, time" points taken from a buildup or drawdown cycle.

The 2014 book also extends the method to transversely isotropic media, an application not covered in Proett, Chin and Chen [11]. In many practical applications, such as infill drilling, hydraulic fracturing and wellbore stability, an understanding of underlying rock anisotropy is important. Thus, engineers prefer separate values for the horizontal and vertical permeability, denoted by k_h and k_v respectively. The extension is important because single-probe methods are limited to predictions for $k_h^{2/3}k_v^{1/3}$, known as the effective, spherical or ellipsoidal permeability k_{eff}. An anisotropic math model is required to explore the variety of pressure interpretation approaches possible. Since the value of a $k_h^{2/3}k_v^{1/3}$ is known, a second relationship connecting k_h and k_v is required. This second relation provides the two equation system needed to determine the two independent permeabilities.

Chin et al. [1] also describes several methods to solve for k_h and k_v. All of these require pressure data from two probes separated axially along the formation tester tool axis. Additional probes, as illustrated in Figure 2, would be desirable; these provide redundancy and support additional measurements using different transducer pairs. Pumping can be executed from a single pumping location at the far left - the observation probe is passive and only records pressure measurements. The predictive methods are summarized next.

(1) In the simplest, *steady-state* drawdown or buildup pressures at both probes, together with dip angle, are required to produce k_h and k_v. This approach is straightforward, however, it may require long wait times in formations with lower mobilities. This implies long, costly wait times and increases the likelihood for stuck tool strings.

(2) A single drawdown may be performed, with flow rate and pressure measured at the pumping nozzle. This leads to predictions for $k_h^{2/3}k_v^{1/3}$. Next, the same sink probe oscillates sinusoidally in time for 2-3 cycles, and the travel-time to an adjacent passive observation probe is measured, say t_{shift}. Knowledge of k_{eff} and t_{shift} are sufficient to determine k_h and k_v.

(3) A single drawdown or buildup is performed at the pumping probe and the pressure at its location is measured. As before, calculations are performed to determine $k_h^{2/3}k_v^{1/3}$. A derived formula for transient pressure at the adjacent observation probe location is available, and depends on k_h and k_v. However, either of k_h or k_v can be eliminated since the value of $k_h^{2/3}k_v^{1/3}$ is known from the source probe test. For the purposes of discussion, we assume that we have eliminated k_v so the altered equation is written only in terms of k_h. Then, this k_h can be adjusted as required to match transient pressure values collected at the observation probe. Once the required k_h is determined, k_v can be calculated since the value of $k_h^{2/3}k_v^{1/3}$ is known.

(4) Finally, k_h and k_v determination is possible by observing how two separate pulses emerging from the sink probe dynamically interact as they travel away in the axial interaction. Examples are given for our "pulse interaction" method in [1], one that again does not require significant

hardware change aside from the introduction of additional passive non-pumping observation probes.

Operationally, (2) requires pump oscillations that may be difficult or inconvenient to perform mechanically. Alternatively, (3) may be preferred because the method does not require additional pump excitations - transient pressures are now measured at the observation probe in addition to that at the sink code. However, one obstacle has prevented implementation of (3) and (4) until now - calculations for observation probe pressure have proven to be difficult, despite the fact that sink probe calculations are routinely performed. We will explain this problem and provide numerical means to overcome the problem.

4.2 Transient Transversely Isotropic Darcy Flow - Forward Solutions for Module FT-00

For transversely isotropic formations, P(x, y, z, t) satisfies an initial-boundary value problem formulation defined by a more complicated differential equation and a velocity flux condition, in particular,

$$k_h\,\partial^2 P(x,y,z,t)/\partial x^2 + k_h\,\partial^2 P(x,y,z,t)/\partial y^2 + k_v\,\partial^2 P(x,y,z,t)/\partial z^2 = (\emptyset\mu c)\,\partial P/\partial t \qquad (1a)$$

$$P(x,y,z,t=0) = P_0 \qquad (1b)$$

$$P\left(\sqrt{x^2+y^2+z^2} \to \infty, t\right) = P_0 \qquad (1c)$$

$$\int q \cdot n\, dS - VC\,\partial P/\partial t = Q(t) \qquad (1d)$$

Uniform pressures are assumed initially, with a level equal to the farfield pore pressure P_0. Here, a horizontal permeability k_h applies in the x and y directions, while a vertical permeability k_v holds along the z coordinate, and t is time. A constant Newtonian viscosity of μ is assumed. These local Cartesian axes refer to the target volume and not to ground fixed coordinates. Equation (1a) describes mass conservation in compressible liquids. Velocity and probe nozzle interactions during pumping are described by Equation (1d) where the integral represents a closed integral over a control surface S surrounding the nozzle and Q(t) is a prescribed unsteady volume flow rate that is associated with actual fluid flow and "VC" expansion effects within the flowline (V represents the flowline volume while C denotes the fluid compressibility in V).

The integrand **q·n** denotes perpendicular components of the Darcy velocity vector **q** = (kh/μ) (∂P/∂x **i** + ∂P/∂y **j**) + (kv/μ) ∂P/∂z **k** acting on S. It reduces to $(4\pi R_w^2 k/\mu)\,\partial P\,(R_w, t)/\partial r$ in isotropic media when $k = k_h = k_v$, spherical symmetry applies and S reduces to a familiar πR_w^2.

We define asterisked dimensionless variables $p^*\,(r^*, t^*) = \{P(x, y, z, t) - P_0\}/P_{ref}$ together with $r^* = \{x^2/k_h + y^2/k_h + z^2/k_v\}^{1/2}$ and $t^* = t/t_{ref}$ so $\partial^2 p^*/\partial r^{*2} + 2/r^*\,\partial p^*/\partial r^* = \phi\mu c/t_{ref}\,\partial p^*/\partial t^*$. In the isotropic limit, a spherical surface "$x^2 + y^2 + z^2 = R_w^2$" would apply noting that R_w is a spherical well radius. For transversely isotropic flow we instead introduce an ellipsoidal surface $x^2/k_h + y^2/k_h + z^2/k_v\}^{1/2} = r^{*}_w{}^2$ with a dimensionless $r^{*}_w = R_w/(k_h^{1/3}k_v^{1/6})$. We also express Q(t) in the form $Q(t) = Q_0\,F(t^*)$. It can be shown that $\int_\Sigma \mathbf{q}\cdot\mathbf{n}\, dS = -(4\pi r^{*}_w{}^2 P_{ref} k_v^{1/2} k_h/\mu)\,(\partial p^*/\partial r^*)_w$ so that

$$\partial^2 p^*/\partial r^{*2} + 2/r^*\,\partial p^*/\partial r^* = \emptyset\mu c/t_{ref}\,\partial p^*/\partial t^* \qquad (2a)$$

$$p^*(r^*, 0) = 0 \tag{2b}$$

$$p^*(r^* \to \infty, t^*) = 0 \tag{2c}$$

$$(4\pi {r^*}_w^2 P_{ref} {k_v}^{1/2} k_h/\mu)(\partial p^*/\partial r^*)_w - VCP_{ref}/t_{ref}\,\partial p^*/\partial t^* = Q_0 F(t^*) \tag{2d}$$

We now select t_{ref} and P_{ref} to normalize the problem so it contains just a single parameter. This is accomplished using a second set of dimensionless variables with *italicized* letters on assuming $p^*(r^*, t^*) = p(r, t)$, $r = ar^*$ and $t = t^*$ where a is dimensionless. Note that the choices $a = 4\pi\phi c k_v^{1/2} k_h {r^*}_w^2/(VC)$, $t_{ref} = \mu V^2 C^2 / (16\pi^2 \phi c k_v k_h^2 {r^*}_w^4)$, $P_{ref} = \phi Q_0 VC / (16\pi^2 \phi c k_v k_h^2 {r^*}_w^4)$ reduce Equations (2a-2d) to the simpler form

$$\partial^2 p/\partial r^2 + 2/r\,\partial p/\partial r = \partial p/\partial t \tag{3a}$$

$$p(r, t = 0) = 0 \tag{3b}$$

$$p(r \to \infty, t) = 0 \tag{3c}$$

$$\partial p(r_w, t)/\partial r - \partial p/\partial t = F(t) \tag{3d}$$

The general solution to this formulation can be obtained by Laplace transforming Equation (3a) in time, and applying the initial condition in Equation (3b). Then the resulting ordinary differential equation is simplified using the regularity condition in Equation (3c) and the pumping description in Equation (3d).

4.2.1 Solution for Constant Rate Drawdown and Buildup

We now provide exact, closed-form, analytical solutions for simple unsteady buildup or drawdown, which can be used to construct general flow rate solutions using Convolution superposition integrals. Suppose $Q(t) = Q_0$ $F(t) = Q_0$ constant, so that $F(t) = 1$, with $Q_0 > 0$ for production and $Q_0 < 0$ for injection. If we define *complex* constants β_1 and β_2 through $\beta_1 = +1/2 - 1/2\sqrt{(1 - 4\,r_w^{-1})}$ and $\beta_2 = +1/2 + 1/2\sqrt{(1 - 4\,r_w^{-1})}$, the dimensionless sink pressure at r_w is given by Equation (4a). This is applicable to all time and ranges of dimensionless parameters. At $r > r_w$ for a second distant observation probe or any position in the formation, the pressure in Equation (4b) applies.

$$p_{exact}(r_w, t) = \{1/(\beta_1 - \beta_2)\} \{{\beta_1}^{-1} - {\beta_1}^{-1} \exp(\beta_1^2 t)\,\mathrm{erfc}(\beta_1\sqrt{t}) - {\beta_2}^{-1} + {\beta_2}^{-1} \exp(\beta_2^2 t)\,\mathrm{erfc}(\beta_2\sqrt{t})\} \tag{4a}$$

$$\begin{aligned} p_{exact}(r, t) = {} & \{r_w/(r(\beta_1 - \beta_2))\} \times \\ & \{\{-exp(\beta_1^2 t - \beta_1(r - r_w))\mathrm{erfc}(\beta_1\sqrt{t} + (r - r_w)/(2\sqrt{t}))] \\ & + erfc((r - r_w)/(2\sqrt{t}))\}/\beta_1 \\ & -\{-exp(\beta_2^2 t - \beta_2(r - r_w))\mathrm{erfc}(\beta_2\sqrt{t} + (r - r_w)/(2\sqrt{t})) \\ & + erfc((r - r_w)/(2\sqrt{t}))\}/\beta_2\} \end{aligned} \tag{4b}$$

The "erfc" appearing in Equations (4a, 4b) is a standard mathematical construct referring to the "complex complementary error function with complex arguments." The source and observation

point pressures in Equations (4a, 4b) are exact, and direct computations would seem to be straightforward.

Nonetheless, implementation issues arose in numerical calculations. One would think that the most challenging efforts should relate to source probe properties where flow gradients are large. However, it is Equation (4b) that proved problematic, since it involved the products of extremely large "L" and extremely small "S" quantities. This was remedied by reformulating the library algorithm so that the finite and well behaved quantity "LS" was handled directly. Successful calculations are shown later in Example 8. Inverse methods for axial probe configurations are presented in Chin et al. [1] where numerous examples are considered. These are based on Equations (4a, 4b). Basically, the relevant equations in the drawdown or buildup cycle are evaluated at three "pressure, time" data points and then solved for three relevant properties using iterative methods.

Other results are more direct and elegant. For instance, compressibilities can be determined using the early time asymptotic solution in Equation (4c), while porosities are found from the intermediate time expansion in Equation (4d). Superpositions draw on the Convolution Integral of Equation (4e), allowing explicit forward and inverse results to be derived for convenient use. Here, the function F represents the dimensionless flow rate. The results of this section are incorporated into algorithm FT-00, which we emphasize is analytically based and without the numerical truncation errors typically associated with artificial viscosity artifacts.

$$\mathrm{P}(\mathrm{R_w},\mathrm{t})_{very-early-time\ from\ exact} \approx \mathrm{P_0} - \mathrm{Q_0 t}/(\mathrm{VC}) \tag{4c}$$

$$\mathrm{P}(\mathrm{R_w},\mathrm{t})_{late-time\ from\ exact} \approx \mathrm{P_0} - \mathrm{Q_0}\mu/(4\pi \mathrm{R_W} {\mathrm{k_h}}^{2/3} {\mathrm{k_v}}^{1/3}) + \{\mathrm{Q_0}\mu/(4\pi \mathrm{k})\}\sqrt{\{\emptyset \mu \mathrm{c}/(\pi {\mathrm{k_h}}^{2/3} {\mathrm{k_v}}^{1/3} \mathrm{t})\}} \tag{4d}$$

$$p_{exact}(r_w,t) = \{1/(\beta_1 - \beta_2)\} \times \int_0^t \mathrm{F}(\tau)\{\beta_2 \exp({\beta_2}^2 (t-\tau))\mathrm{erfc}\beta_2\sqrt{(t-\tau)} - \beta_1 \exp({\beta_1}^2 (t-\tau))\mathrm{erfc}\beta_1\sqrt{(t-\tau)}\}\mathrm{d}\tau \tag{4e}$$

4.3 Observations on Transient Isotropic Darcy Flow

The full mathematical foundations for "ideal source" modeling were developed in Chin et al. [1] almost two decades after its commercial use in Proett, Chin and Chen [11]. While the methods were broad, with several applying to "inverse problems," actual applications were limited for years because certain standard math library routines were not robust. These problems were remedied by modifying the erfc algorithm as noted above. Again, the "forward problem" refers to pressure versus time calculations when input parameters like permeability, compressibility, porosity and others are given. The "inverse problem" determines these parameters when pressure values are available, usually from measured data, at a limited number of discrete time points.

In petroleum exploration, forward or "direct" solutions provide engineers with useful "job planning" information, for properties prediction, e.g., the time needed (based on crude permeability estimates) for formation tester pressure measurements to more accurately characterize permeability, compressibility, porosity and pore pressure. Well logging times are

important because onshore and offshore drilling rig rentals are costly; moreover, the longer the formation tester spends in acquiring data, the greater the risk of "stuck tools that are lost" - that is, expensive tools that cannot be removed mechanically due to mudcake adhesion.

Inverse or "indirect" solutions for the cited properties are important for several reasons. Among these, "anisotropy" ranks among the most important, a quantity defined by the ratio of horizontal to vertical permeabilities k_h/k_v. This parameter plays a prominent role in hydraulic fracturing, infill drilling and wellbore stability. However, single-probe formation testers can measure only the effective permeability $k_{eff} = k_h^{2/3}k_v^{1/3}$ at best (it can be shown that the usual constant permeability "k" in an isotropic formation is identical to k_{eff} in a transversely isotropic medium). We have shown that it is possible to determine horizontal and vertical permeability independently using a math model that fully accounts for transversely isotropic flow effects.

The above forward solution, solving for pressure when input parameters for tool, formation and pump schedule are prescribed, satisfies the exact, analytical, closed form expressions shown, which were first published in Chin et al. [1]. These also provided the foundation for subsequent inverse methods, which predict problem parameters when values of pressure at specific locations are available at different times.

4.4 Typical Axial Array Evaluation Example

Useful array formation testers require careful design and detailed understanding of the flow behavior as it depends on input parameters. Computer models provide the platform necessary for parametric "what if" studies. We emphasize that central to our approach is an exact, analytical solution to the complete Darcy flow formulation that is free of numerical truncation errors. Commercial simulators rely on finite difference and finite element methods, for which "artificial viscosity" effects are well documented. For example, this means that the output associated with a 10 md/cp input may in fact behave like 5 or 15 md/cp or another value, and that trend results may vary with volume flow rate and other parameters. The forward pressure solver FT-00, because it is based on analytical, exact, closed form results, provides rapid and accurate solutions. These are always automatically plotted and tabulated for any inputs assumed in Figure 19a. Detailed calculations appear in Chin et al. [1].

Multiple simulations in which input quantities are systematically varied may be performed from the "Batch Runs" command at the upper left of Figure 20. In fact, automated runs for any two input parameters may be programmed to operate with nested do-loop convenience. On the other hand, the "Run" button at the bottom right activates an auxiliary solver that rapidly calculates and plots pressure versus time solutions at multiple transducer locations for a prescribed set of fluid and formation input parameters. A sample run is shown in Example 8.

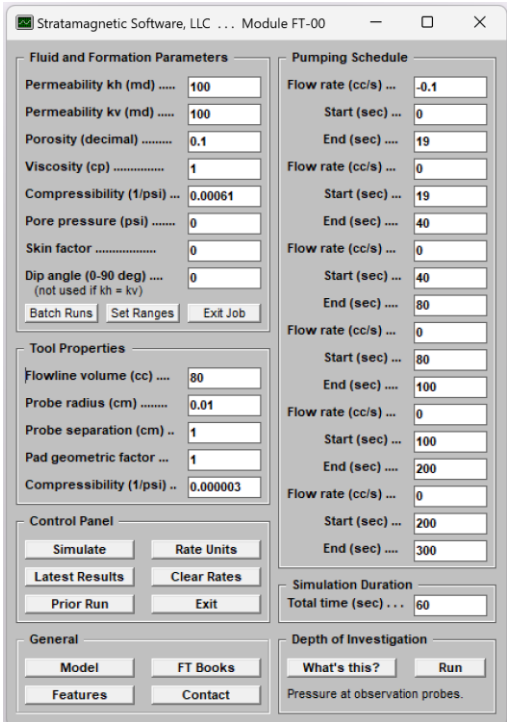

Figure 20 Exact FT-00 forward pressure simulator, with output for pumping sink (source) probe and one additional passive observation probe.

4.4.1 Example 8 Time-Wise Pressure Histories at Different Axial Probe Locations.

Figure 21 illustrates one calculation, showing how the time-wise source pressure signal attenuates and disperses as it propagates away. This information guides the choice of pulses that lead to clear and discernible pressures useful for input to inverse properties prediction algorithms. Pulse design is optimized by use of Module FT-00, whose menu is shown above, with detailed computed results described in Chin et al. [1].

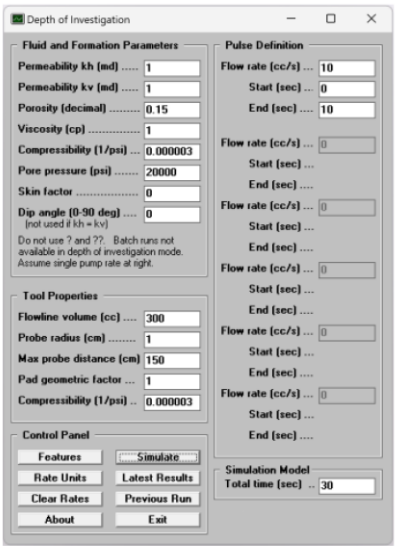

(a) Axial transducer input menu, single source probe.

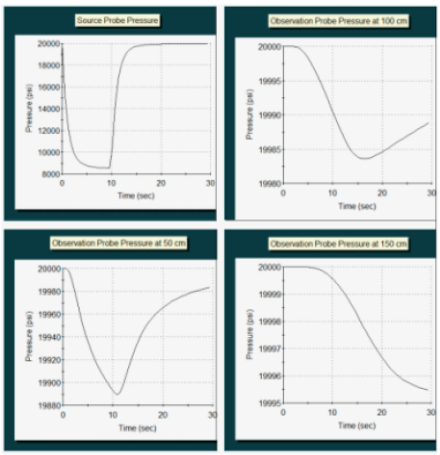

(b) Pressure waveforms at different observation locations.

Figure 21 Axial pulse propagation.

5. Conclusions and Closing Remarks

During the 1990s and early 2000s, two types of formation testers prevailed. The first class is represented by "single probe tools," where pumping and pressure observation functions are both performed at a single location. The second is represented by "dual probe tools" in which a first probe pumps, while the second, located a short distance axially away along the same azimuth, passively observes and only records pressures. The probes themselves may consist of small "round or oval nozzles," or possibly, "long slotted nozzles." The former are reserved for solid matrix rock, whereas the latter are intended for formations characterized by small fractures or looser unconsolidated sands. In all cases, nozzles are surrounded by hard rubber pads which seal the formation away from borehole invasion due to higher pressure mud flow.

In this paper, we have provided an overview of a new "three arm" *azimuthal array formation tester* that provides enhanced capabilities over the conventional tools described above. In particular, we gave illustrations of China Oilfield Services Limited's (COSL) "triple probe" tool in Figure 1. Other commercial multiprobe tools are available. These include Schlumberger's MDT™, Saturn™ and ORA™, while patented Halliburton (U.S. Patent 10,738,607) and BakerHughes (U.S. Patent 9,777,572) concepts will be commercially available shortly. Aside from the MDT™, which consists of two azimuthal probes 180 deg apart, the remainder are four-probe tools, possibly augmented by addition rows of four-probe "focusing" arrays just short axial distances away. Focusing functions, important to invasion contamination remediation, are not discussed here, but will form the subject of the book in Chin [6].

The MDT™, which again consists of diametrically opposite probes, is known for sub-optimal signal detection at its 180 deg displaced observation probe. This results from high levels of attenuation in lower mobility formations. Azimuthal multiprobe tools remedy this problem by introducing additional probes. The advantages behind the COSL tool are several. (1) Closer 120 deg probe spacings better support formation evaluation in low permeability environments, especially where 180 deg separations suffer from excessive pressure attenuation. (2) Detailed studies interestingly show that four azimuthal probes may be excessive, in a certain sense decreasing measurement sensitivity. This arises because additional formation "real estate" is needed to host the fourth nozzle, thus reducing the formation volume available for pressure measurement.

Next, (3) Multiprobe probes that operate independently, with possibly different nozzle shapes and different flow rate schedules, that is, rate, start and stop times, improve tool capabilities in identifying formation heterogeneities - they can "see" simultaneously in different directions with different depths of investigation. (4) Tool design has been guided by the use of state-of-the-art simulation capabilities, which fully account for borehole size and probe interactions. These are useful in job planning applications, e.g., estimating the measurement times required to collect pressure data for accurate inverse evaluation. (5) Finally, rigorous azimuthal models such as those described form the basis of inverse capabilities for permeability and pore pressure prediction, plus large databases for real-time machine learning applications.

Axial probe formation tester arrays were also discussed in this paper. While the "dual probe" device discussed above does represent the smallest axial array tester possible, we generally use the "array" designation to describe tools as shown in Figures 2 and 3. Measurement differences between different probes can be explained physically in terms related to "depth of investigation" and "vertical resolution," analogously to how these terms are presently used in resistivity or

electromagnetic logging. In Figure 21, we gave calculations using extensions of a method developed originally in Chin et al. [1]. The detailed formation information available in such pressure traces is useful in evaluating anisotropy ratios as well as changes in anisotropy along the formation tester axis.

Figure 22 conceptually describes a "hybrid, mixed probe" formation tester under design at COSL. The diagram shown displays a "triple-probe" device at the far left. A "slotted nozzle" is given at the center, while assorted smaller round and oval nozzles are given at the right. It is impossible to list all of the separate combinations of probes possible - these depend on the well logging objectives and the engineer's initial views of the geology. Again, azimuthal multiprobe tools "see" circumferentially, while "axial arrays," located along the formation tester tool axis, see changes in the vertical direction (for wireline operations) and also detect pressure gradients and pressure discontinuities indicating isolated formations.

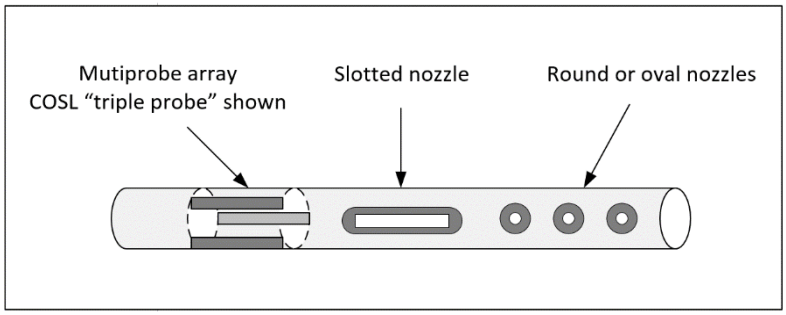

Figure 22 Conceptual "mixed probe" formation tester.

The computational solutions offered in this article allow detailed studies for both azimuthal and axial multiprobe array formation testers. These methods solve the "forward problem," that is, they solve for the transient, spatial pressure field once input parameters for fluid, rock and tool properties are given. However, they do not address the "inverse problem," in which permeability, compressibility, pore pressure and porosity are sought when pressures are available at selected time points at a fixed location (these will be addressed in detail in Chin [6]). However, solutions to the forward problem are essential to inverse algorithm development in the follow manner. Approximate inverse models are used, during validation, to recover the input parameters used in generating detailed exact synthetic forward solutions - if there is agreement, then the models are credible. In addition, well formulated forward solvers can be used to generate large databases useful in artificial intelligence and machine learning applications. This underlies the philosophy behind "AI with physics" approaches. Inverse problems, rapid solutions, nonlinear gas pumping, in addition to those for multiphase flow contamination due to mud invasion, again, will be considered in Chin [6]. A complimentary draft copy of this publication is available to readers upon request.

Author Contributions

Minggao Zhou leads the formation testing project team. He has worked extensively in the research, development, promotion and technical support of formation testing instruments. Yongren Feng is mainly responsible for wireline formation testing, electric core sampling and formation testing while drilling technologies. Yongzeng Xue holds a Master's Degree and is an

Intermediate Electronics Engineer. He is engaged in research and development on the formation testing project team, and has worked extensively in the design of formation testing instrument control circuits and in technical support. Yanmin Zhou has participated in the Drilling and Reservoir Testing Instrument Development Program, the National Science and Technology Special Project, and acts as R&D engineer in national formation testing activities. Yongchao Chen active in the research and development of formation testing instruments. He is engaged in analysis, design and trouble-shooting of mechanical prototypes and provides on-going technical support for project activities. Wilson Chin developed the algorithms described and authored the manuscript.

Competing Interests

The authors have declared that no competing interests exist.

Acronyms and Nomenclature

1. Acronyms

CFD	Computational fluid dynamics
COSL	China Oilfield Services Limited
FT-00	Exact solution solver for formation testing forward modeling
MDT	Trademark of Schlumberger (formation tester)
ORA	Trademark of Schlumberger (formation tester)
Saturn	Trademark of Schlumberger (formation tester)

2. Nomenclature

ϕ	Porosity
k_h	Horizontal permeability
k_v	Vertical permeability
θ	Azimuthal angular coordinate
μ	Fluid viscosity
c	Liquid fluid and formation compressibility
C	Flowline compressibility
P	Darcy pressure in the formation
Q	Volume flow rate
V	Flowline volume
x	Horizontal rectangular coordinate
y	Horizontal rectangular coordinate
z	Vertical (axial) coordinate
r	Cylindrical radial coordinate
t	Time coordinate

References

1. Chin WC, Zhou Y, Feng Y, Yu Q, Zhao L. Formation Testing: Pressure Transient and Contamination Analysis. Hoboken, NJ: John Wiley & Sons; 2014.
2. Chin WC, Zhou Y, Feng Y, Yu Q. Formation testing: Low mobility pressure transient analysis. Hoboken, New Jersey: John Wiley & Sons; 2016.
3. Chin WC. Formation Testing: Supercharge, Pressure Testing, and Contamination Models. Hoboken, New Jersey: John Wiley & Sons; 2019.
4. Lu T, Qin X, Feng Y, Zhou Y, Chin WC. Supercharge, Invasion, and Mudcake Growth in Downhole Applications. Hoboken, New Jersey: John Wiley & Sons; 2021.
5. Lu T, Zhou M, Feng Y, Yang Y, Chin WC. Multiprobe Pressure Analysis and Interpretation. Hoboken, New Jersey: John Wiley & Sons; 2021.
6. Chin WC. Multiprobe Pressure Analysis and Reservoir Characterization. Amsterdam: Elsevier Scientific Publishing; 2024.
7. Proett MA, Bonavides CS. Downhole formation testing and sampling apparatus having a deployment linkage assembly. Houston, TX, US: Halliburton Energy Services; 2020; 10,738,607.
8. Morgan CJ, Nieuwoudt HJ, Cernosek JT. Multiprobe Sampling Device. Houston, TX, US: BakerHughes; 2017; 9,777,572.
9. Ma T, Peng N, Chen P, Yang C, Wang X, Han X. Study and verification of a physical simulation system for formation pressure testing while drilling. Geofluids. 2018; 2018: 1731605.
10. Lee HJ. Simulation and interpretation of formation-tester measurements acquired in the presence of mud-filtrate invasion and geomechanical deformation, Doctoral Thesis. Austin, TX, US: The University of Texas at Austin; 2008.
11. Proett MA, Chin WC, Chen C. Method of formation testing. United States Patent 5,703,286, Halliburton Energy Services, Houston, TX, US; 1997.
12. Chin WC, Proett MA. Formation tester immiscible and miscible flow modeling for job planning applications. Proceedings of the 46th Annual SPWLA Meeting; 2005 June 26-29; New Orleans, LA. Houston, TX, US: SPWLA.
13. Rourke M, Powell B, Platt C, Hall K, Gardner A. A new hostile environment wireline formation testing tool: A case study from the Gulf of Thailand. SPWLA 47th Annual Logging Symposium; 2006 June 4-7; Veracruz, Mexico. Houston, TX, US: SPWLA.
14. Halliburton Staff. Testing the Tight Gas Reservoir: Hostile-Environment Wireline Formation Tester Reduces NPT in HPHT Boreholes [Internet]. Houston, TX, US: Halliburton; 2018. Available from: https://www.halliburton.com.